JM PAPERS

Unified analytical solution for group-induced infragravity waves based on Green's function

Zhiling Liao[1,2], **Qingping Zou**[2,†], **Ye Liu**[1,†], **Stephanie Contardo**[3] **and Shaowu Li**[1]

[1]State Key Laboratory of Hydraulic Engineering Simulation and Safety, Tianjin University, Tianjin 300072, PR China

[2]The Lyell Centre for Earth and Marine Science and Technology, Institute for Infrastructure and Environment, Heriot-Watt University, Edinburgh EH14 4AS, UK

[3]CSIRO Environment, Crawley, Western Australia 6009, Australia

Short-wave group forcing is a major driving mechanism of infragravity waves. The subharmonic response to wave group forcing approaches resonance in shallow water where the group velocity is equal to the shallow-water wave-propagating speed. Currently, there is a lack of understanding of the connection between the free and bound components of group-induced infragravity waves and the consistency among existing solutions for off- and near-resonance conditions in intermediate and shallow water. Here, a unified solution of group-induced subharmonics is derived based on Green's function for the first time. The new solution is valid for any resonance intensity and is able to describe group-induced subharmonic behaviour at all water depths consistently from a new angle. The proposed solution reduces to existing solutions for intermediate depth (Longuet-Higgins & Stewart, *J. Fluid Mech.*, vol. 13, 1962, pp. 481–504; Zou, *Phys. Oceanogr.*, vol. 41, 2011, pp. 1842–1859), shallow water and/or over a plane sloping beach (Van Leeuwen, PhD thesis, TU Delft, 1992; Schäffer, *J. Fluid Mech.*, vol. 247, 1993, pp. 551–588; Janssen *et al.*, *J. Geophys. Res.*, vol. 108, 2003, p. 3252; Contardo *et al.*, *J. Phys. Oceanogr.*, vol. 51, 2021, pp. 1465–1487; Liao *et al.*, *J. Phys. Oceanogr.*, vol. 51, 2021, pp. 2749–2765). Unlike previous solutions, the Green's function-based solution describes all subharmonics as free subharmonics continuously radiated away from each point source in the group-induced forcing field determined by wave radiation stress gradients. The superposition of all these free subharmonics yields so-called bound subharmonics by previous studies due to group-modulated emission of each free subharmonic through the source field bound to the wave group. Therefore, this solution provides theoretical evidence that the group-induced subharmonic at any observation point is dependent on the surrounding radiation stress field

† Email addresses for correspondence: q.zou@hw.ac.uk, liuye2009@tju.edu.cn

and topography. Under full-resonance conditions in shallow water, downwave-propagating subharmonics excited at all source locations interfere with each other constructively; therefore, their superposed amplitude is proportional to the travel distance of wave groups. Combined with the conventional moving-breakpoint forcing model, the predicted amplitude of the subharmonic in the surf zone by the present solution is in good agreement with laboratory observations.

Key words: surface gravity waves

1. Introduction

Infragravity waves of frequency 0.004–0.04 Hz were first identified outside the surf zone by Munk (1949) and Tucker (1950) from field observations. Since then, numerous researches have confirmed that infragravity waves can be a dominant forcing factor for nearshore water motion (Stockdon *et al.* 2006), coastal inundation (Cheriton, Storlazzi & Rosenberger 2016; Henderson *et al.* 2022) and sediment transport (Roelvink *et al.* 2009; Palmsten & Splinter 2016). Infragravity waves may cause resonant response of harbours (Diaz-Hernandez *et al.* 2015), marine structures (Zhao *et al.* 2022) and ice shelves (Bromirski *et al.* 2017). Readers are referred to Bertin *et al.* (2018) for a full review of the generation mechanisms and impacts of infragravity waves.

A ubiquitous mechanism for the generation of nearshore infragravity waves is the second-order nonlinear forcing of short-wave groups. Longuet-Higgins & Stewart (1962) (hereafter referred to as LHS62) showed that infragravity waves of the scale of short-wave groups are induced by nonlinear group forcing through the wave radiation stress gradient. Study LHS62 provided an equilibrium solution for one-dimensional (1-D) group-induced infragravity waves on a flat bottom, which is the bound subharmonic in antiphase with the group. The equilibrium solutions for the two-dimensional counterpart were proposed by Hasselmann (1962) and McAllister *et al.* (2017).

As wave groups propagate over variable depth, however, the equilibrium solution is no longer valid. For instance, with diminishing depth on a sloping beach towards the shore, the incident bound infragravity waves increasingly lag behind wave groups and gain more energy through nonlinear interaction with wave groups outside the surf zone, as observed in laboratory experiments (Van Leeuwen 1992; Janssen, Battjes & van Dongeren 2003; Guérin, de Bakker & Bertin 2019), numerical modelling (List 1992; Melito *et al.* 2022; Liu *et al.* 2023) and field experiments (Elgar & Guza 1985; Masselink 1995; Contardo & Symonds 2013; Inch *et al.* 2017). This process of energy transfer from primary waves to infragravity waves is subject to offshore wave conditions and tidal modulation of local depth (Thomson *et al.* 2006; Bertin *et al.* 2020) even in a microtidal environment (Melito *et al.* 2022). The key indicator of the occurrence of energy transfer is the non-equilibrium phase coupling between infragravity waves and wave groups due to the presence of additional infragravity waves that lag the equilibrium bound subharmonic by $\pi/2$. In intermediate water, the additional wave manifests itself as a bound subharmonic induced by the perturbation of the bottom slope (Bowers 1992; Van Leeuwen 1992; Janssen *et al.* 2003; Zou 2011); in shallow water, it is interpreted as a free subharmonic (Mei & Benmoussa 1984; Nielsen & Baldock 2010; Moura & Baldock 2019; Contardo *et al.* 2021). Free infragravity waves can also be generated in the surf zone as dynamic wave-induced set-up through the moving-breakpoint forcing mechanism (Symonds, Huntley & Bowen 1982; Contardo, Symonds & Dufois 2018).

For wave groups in intermediate water depth over a mildly sloping bottom, Janssen *et al.* (2003) and Zou (2011) obtained analytical solutions to the 1-D linearised shallow water equation with a forcing term of radiation stress curvature through the perturbation approach. The off-resonant solution of Janssen *et al.* (2003) shows that the phase lag of the infragravity wave with respect to group forcing shifts away from π toward 1.5π as depth decreases. Using a multiscale Wentzel–Kramers–Brillouin expansion method, Zou (2011) proposed a second-order analytical solution that is the sum of an equilibrium bound subharmonic described by the LHS62 solution for flat bottom, a topography-induced bound subharmonic in quadrature with the LHS62 solution and two free subharmonics propagating in opposite directions due to scattering at the edge of finite topography.

As the group propagating velocity approaches the free long-wave propagating velocity in shallow water, resonance occurs between group forcing and subharmonics propagating in the same direction as wave groups, causing the solutions based on the perturbation method to diverge. In this case, implicit solutions in integral form were derived by Symonds *et al.* (1982), Van Leeuwen (1992) and Schäffer (1993) for a plane beach, and by Liao *et al.* (2021) for arbitrary topography with a mildly sloping bottom. The near-resonant solution of Liao *et al.* (2021) indicates that, with diminishing depth on a plane beach, the group-induced subharmonic asymptotically leads the group forcing by $\pi/2$ at leading order, and its amplitude increases as $\propto h^{-1}$ (h = depth), a shoaling rate lower than the shallow-water limit of the LHS62 solution ($\propto h^{-2.5}$) but higher than the free infragravity wave growth rate ($\propto h^{-0.25}$, known as Green's law; Green 1838). Contardo *et al.* (2021) (hereinafter CLHRDS21) proposed an alternative solution for shallow water of variable depth, by discretising the topography into many steps, and applying the LHS62 solution on both sides of each step to derive the free subharmonics scattered due to the abrupt depth change. Study CLHRDS21 derived the total subharmonic as the superposition of the local bound subharmonic given by the LHS62 solution and the free subharmonics scattered from all the steps through which the wave groups have travelled.

However, the transition of group-induced subharmonic from weak resonance in intermediate depth to strong resonance in shallow water is currently not well understood, because there is no clear dividing line between the parameter regimes of the above-mentioned models. This deficit directly leads to a debate on the releasing process of bound subharmonics in shallow water. More specifically, it is often assumed that the group-bounded subharmonic is released when the primary waves begin to break (e.g. Masselink 1995; Bertin *et al.* 2018), while Baldock (2012) argued that it is released when the group velocity equalled shallow water wave velocity so that resonance occurs, regardless of wave breaking. In addition to the releasing condition, the underlying mechanism for the transition from bound subharmonic to free mode during the releasing process also remains unclear.

To understand the mutual transition between group-induced subharmonics in weak and strong resonance, it is necessary to unify the aforementioned theoretical solutions in order to provide a holistic view of the physical process of the generation of group-induced subharmonics at all water depths. Although the general form of the solution for group-induced subharmonics over 1-D topography was derived by Schäffer (1993) by the method of variation of parameters (equation (4.10) therein), it was only applied to the special case of bichromatic waves normally incident on a plane beach, leaving its consistency with existing solutions and, more importantly, its physical interpretation unaddressed. This issue is crucial for understanding the behaviour of group-induced

subharmonics at all water depths, which forms the motivation and focus of the present study.

In the present work, the solution of group-induced subharmonics is derived based on the Green's function method for the first time, which allows for a novel consistent physical interpretation of generating mechanisms of group-induced subharmonics at all water depths. Green's function is the response function of a linear system to a unit forcing at a point in space or time (Duffy 2015). It is a flexible and powerful mathematical tool for solving non-homogeneous linear differential equations. The forcing term of the equation is treated as spatially distributed unit point forcing weighted by local forcing and thus the response is the weighted linear superposition of responses to all unit point forcing. Green's function has been applied in a wide range of problems related to water waves, including harbour resonance (Miles 1974), internal waves (Voisin 1991), waves over continental shelf (Miles 1972), wave–structure interactions (Telste & Noblesse 1986; Wang, Ning & Zou 2020) and numerous studies based on the boundary element method (e.g. Longuet-Higgins & Cokelet 1976; Liu *et al.* 2011; Ning *et al.* 2015; Zheng *et al.* 2020). Using the present generalised solution proposed, existing solutions (Longuet-Higgins & Stewart 1962; Van Leeuwen 1992; Schäffer 1993; Janssen *et al.* 2003; Zou 2011; Contardo *et al.* 2021; Liao *et al.* 2021) for non-breaking waves are unified. Physically, the solution treats the group-forcing field as a sum of force pulses distributed in time and space, which constantly emit free waves away from each spatial point in the wave field. It is shown that the group-induced subharmonic, previously taken as the sum of bound and free subharmonics, may be interpreted as the results of the emission, propagation and interference of all the free subharmonics generated by the point forcing in the domain.

In the following, we first describe the problem considered and introduce the governing equations in § 2. In § 3, the unified solution of the group-induced subharmonic is derived based on Green's function, along with the physical interpretation of its behaviour in intermediate and shallow water. Unification of existing solutions through the present solution is shown in § 4. Discussions on the generation and formation of group-induced subharmonic from the perspective of Green's function, the influence of topography, the effect of moving-breakpoint forcing and possible extensions of the solution are presented in §§ 5 and 6. Main conclusions are drawn in § 7.

2. Governing equations

By introducing the concept of radiation stress to represent the phase-averaged residual momentum flux due to the presence of waves, LHS62 proposed the theory of low-frequency subharmonic induced by the nonlinear group forcing of radiation stress. For regular waves under non-breaking conditions, the radiation stress S accurate to second order in wave steepness is expressed as (Longuet-Higgins & Stewart 1960)

$$S = E\left(\frac{2c_g}{c} - \frac{1}{2}\right), \tag{2.1}$$

where E denotes the wave energy, c_g is the wave group velocity and c is the wave phase speed.

Consider a unidirectional bichromatic wave group propagating in the positive direction of x with the surface elevation

$$\eta(x, t) = \tfrac{1}{2}A(x, t) \, e^{i\left(\int^x k \, dx' - \omega t\right)} + \text{c.c.}, \tag{2.2}$$

where

$$A (x, t) = A_1 (x) \ e^{\frac{i}{2} \left(\int^x k_g \, dx' - \omega_g t \right)} + A_2 (x) \ e^{-\frac{i}{2} \left(\int^x k_g \, dx' - \omega_g t \right)}, \tag{2.3}$$

A_1 and A_2 are the real amplitudes of the two wave components; $A(x, t)$ is the slowly varying modulated complex amplitude; k and ω are the wavenumber and radian frequency of the short wave; k_g and ω_g are the wavenumber and radian frequency of the wave group; and c.c. denotes the complex conjugate and will be omitted hereinafter. Assuming that the two wave frequencies are close to each other, substituting (2.3) into the equation of wave energy

$$E(x, t) = \tfrac{1}{2} \rho g \left| A(x, t) \right|^2, \tag{2.4}$$

where g is the gravitational acceleration and ρ is the water density, gives

$$E(x, t) = \tfrac{1}{2} \rho g \left[A_1^2(x) + A_2^2(x) + 2 A_1(x) A_2(x) \cos \left(\int^x k_g \, dx' - \omega_g t \right) \right]. \tag{2.5}$$

Equation (2.5) can be decomposed into a steady component and an unsteady oscillatory component. With the cos function expressed in complex form, the oscillatory wave energy is given by

$$\tilde{E} (x, t) = \tfrac{1}{2} \rho g A_1 (x) A_2 (x) \exp \left(i \left(\int^x k_g \, dx' - \omega_g t \right) \right). \tag{2.6}$$

Assuming negligible breaking and bottom-friction-induced dissipation which may have a significant effect on wave radiation stress (Zou, Bowen & Hay 2006), the evolution of wave energy is governed by (see (2.6) in Mei & Benmoussa (1984) and (2.4a) in Zou (2011))

$$\frac{\partial}{\partial t} E + \frac{\partial}{\partial x} \left(c_g E \right) = 0, \tag{2.7}$$

and substituting (2.5) into (2.7), we have

$$A_1^2 + A_2^2 = \frac{[(A_1^2 + A_2^2) c_g]_0}{c_g}, \quad A_1 A_2 = \frac{(A_1 A_2 c_g)_0}{c_g}, \tag{2.8a,b}$$

where the subscript 0 denotes quantities at the incoming boundary of waves.

Substituting (2.6) into to (2.1) yields the oscillating component of the radiation stress:

$$\tilde{S} (x, t) = \tfrac{1}{2} \hat{S} (x) \, e^{-i \omega_g t}, \tag{2.9}$$

where

$$\hat{S} (x) = \rho g A_1 A_2 \left(\frac{2 c_g}{c} - \frac{1}{2} \right) \exp \left(i \int^x k_g \, dx' \right) = \left| \hat{S} (x) \right| \exp \left(i \int^x k_g \, dx' \right). \tag{2.10}$$

Substituting (2.8b) into (2.10), we obtain

$$\left| \hat{S} (x) \right| = \rho g \left(A_1 A_2 c_g \right)_0 \left(\frac{2}{c} - \frac{1}{2 c_g} \right). \tag{2.11}$$

Following LHS62 (equations (3.33) and (3.34) therein), the 1-D linearised mass and momentum conservation equations for the subharmonic under the forcing of radiation
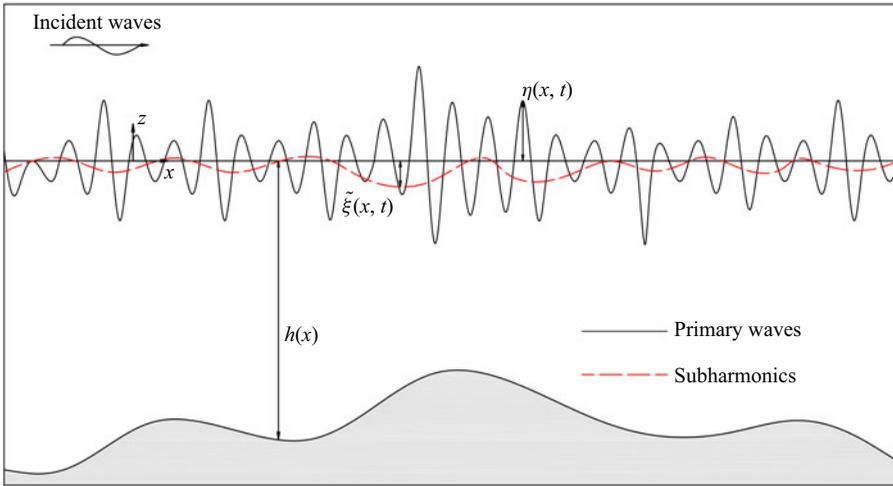
Figure 1. Definition sketch of variables for wave groups propagating over variable bottom.

stress are

$$\rho \frac{\partial \tilde{\xi}}{\partial t} + \frac{\partial \tilde{M}}{\partial x} = 0, \tag{2.12}$$

$$\frac{\partial \tilde{M}}{\partial t} + \rho g h \frac{\partial \tilde{\xi}}{\partial x} = -\frac{\partial \tilde{S}}{\partial x}, \tag{2.13}$$

where $\tilde{\xi}(x, t)$ and $\tilde{M}(x, t)$ are the surface elevation and mass flux of the subharmonic, respectively, and h is the still water depth (see figure 1 for the definition of variables). Equations (2.12) and (2.13) are equivalent to the linearised equations (2.1) and (2.2) in Schäffer (1993). Eliminating $\tilde{M}$ in (2.12)–(2.13) yields

$$\frac{\partial^2 \tilde{\xi}}{\partial t^2} - g \frac{\partial}{\partial x} \left(h \frac{\partial \tilde{\xi}}{\partial x} \right) = \frac{1}{\rho} \frac{\partial^2 \tilde{S}}{\partial x^2}. \tag{2.14}$$

Equation (2.14) is the governing equation of the surface elevation of group-induced subharmonics for 1-D wave groups propagating over a depth small compared with the wave group length (Longuet-Higgins & Stewart 1962). For non-breaking waves outside the surf zone, (2.9)–(2.11) are adopted, and (2.14) is consistent with the governing equation (2.11) in Mei & Benmoussa (1984), equation (7) in Janssen *et al.* (2003) and equation (2.7) in Zou (2011). For breaking waves in the surf zone, Symonds *et al.* (1982) and Schäffer (1993) adopted the saturated breaking model assuming the wave height is proportional to local depth to model the forcing term and then solved equation (2.14), but no satisfactory verification against experiment has been reported. Using numerically modelled flow field to calculate the radiation stress, Rijnsdorp, Smit & Guza (2022) showed that the linearised equation (2.14) remains adequate in the outer surf zone. Furthermore, Rijnsdorp *et al.* (2022) demonstrated that the nonlinearity of infragravity wave itself starts to become important only in the inner surf zone over a mildly sloping beach of bottom slope 1/100. Liu *et al.* (2023) showed that fully nonlinear analysis of the infragravity wave energy budget is required for reef topography where the depth sharply reduces when offshore waves propagate over the foreslope into the reef flat.

967 A37-6

The group-induced subharmonic surface elevation $\tilde{\tilde{\xi}}(x, t)$ oscillates in time with the same frequency ω_g as the wave radiation stress $\tilde{S}$ in (2.9), i.e.

$$\tilde{\tilde{\xi}}(x, t) = \tfrac{1}{2}\hat{\xi}(x)\, e^{-i\omega_g t}, \tag{2.15}$$

where $\hat{\xi}$ is the complex amplitude of $\tilde{\tilde{\xi}}(x, t)$. Substituting (2.9) and (2.15) into (2.14), we obtain the governing equation for the subharmonic complex amplitude $\hat{\xi}(x)$:

$$\frac{1}{h}\frac{d}{dx}\left(h\frac{d\hat{\xi}}{dx}\right) + k_f^2\hat{\xi} = -\frac{1}{\rho g h}\frac{d^2\hat{S}}{dx^2}, \tag{2.16}$$

where $k_f = \omega_g/\sqrt{gh}$ is the wavenumber of free subharmonics propagating at the speed of shallow-water wave. Equation (2.16) is consistent with the governing equation (4.9) in Schäffer (1993), equation (10) in Janssen *et al.* (2003) and equation (3.4) in Zou (2011). A novel unified solution to (2.16) is developed based on Green's function in the present study.

3. Unified solution based on Green's function

3.1. *General form of solution*

The Green's function $G(x, y)$ of a 1-D linear differential equation describes the response at x to a unit forcing at y, where x and y denote two spatial coordinates in 1-D space. Assuming a continuously varying water depth $h(x)$, the governing equation (2.16) becomes a Sturm–Liouville type equation. The corresponding Green's function satisfies (see equations (3.3.6), (3.3.9) and (3.3.10) in Duffy 2015) the following equations:

$$\frac{1}{h}\frac{d}{dx}\left[h\frac{d}{dx}G(x, y)\right] + k_f^2 G(x, y) = \delta_{Dirac}(x - y), \tag{3.1a}$$

$$\lim_{x \to y^-} G(x, y) = \lim_{x \to y^+} G(x, y), \tag{3.1b}$$

$$\lim_{x \to y^+}\frac{\partial G(x, y)}{\partial x} - \lim_{x \to y^-}\frac{\partial G(x, y)}{\partial x} = 1, \tag{3.1c}$$

where $\delta_{Dirac}(x - y)$ is the Dirac Delta function that physically describes the unit point forcing oscillating at the wave group frequency at $x' = x - y = 0$ and satisfies $\delta_{Dirac}(x') = 0$ for $x' \neq 0$ and $\int_{-\infty}^{+\infty}\delta_{Dirac}(x')\, dx' = 1$. An example of $G(x, y)$ over a flat bottom is later shown in figure 3.

Let $\hat{f}(x)$ be the complex amplitude of the forcing term of (2.16), i.e.

$$\hat{f}(x) = -\frac{1}{\rho g h}\frac{d^2\hat{S}}{dx^2}. \tag{3.2}$$

For any given response position x, we can always find a subdomain $a < x < b$ where the equality

$$\hat{f}(x) = \int_a^b \hat{f}(y)\, \delta_{Dirac}(x - y)\, dy \tag{3.3}$$
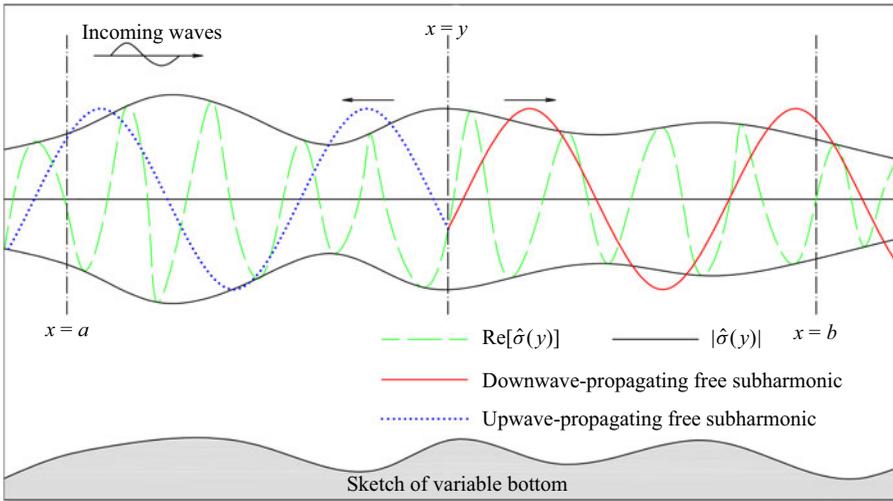
is valid.

Figure 2. Diagram of two downwave-propagating (red) and upwave-propagating (blue) free subharmonics emitted from an arbitrary spatial point $x = y$ in the source field $\hat{\sigma}(y)$ (3.7) due to group forcing. The source field $\hat{\sigma}(y)$ due to the forcing of radiation stress varies at the spatial scale of wave group length (see (3.22) for an example). The superposition of all the free subharmonics emitted everywhere yields the group-induced subharmonic.

Applying the multiplication and then integration on the right-hand side of (3.3) to both sides of (3.1a) and comparing with the governing equation of subharmonic complex amplitude (2.16), the inhomogeneous solution $\hat{\xi}_g(x)$ to (2.16) is found in the form of

$$\hat{\xi}_g(x) = \int_a^b \hat{f}(y)\, G(x, y)\, \mathrm{d}y, \qquad (3.4)$$

which physically describes the group-induced subharmonic at x as the linear superposition of the responses at x induced by all the wave group forcing $\hat{f}(y)$ distributed in the domain $a < y < b$. The generalised solution to (2.16) can be constructed as the sum of homogeneous and inhomogeneous components (cf. Ince 1956, § XI):

$$\hat{\xi}(x) = \hat{\xi}_g(x) + \hat{\xi}_f(x), \qquad (3.5)$$

where the homogeneous solution $\hat{\xi}_f(x)$ denotes the free infragravity wave that satisfies the homogeneous counterpart of governing equation (2.16). Physically, the response to each point forcing $\hat{f}(y)$ over $a < y < b$ propagates away from the source point $x = y$ as free subharmonics (figure 2), because (3.1a) indicates that $G(x, y)$ is the homogeneous solution to (2.16) at all x in the domain except for $x = y$. Therefore, (3.4) shows that the group-induced subharmonic at an observation point x is the linear superposition of free subharmonics generated from all source points $x = y$ in the wave field due to local group forcing. Note that, at the observation position x within this domain, the response to group forcing outside this domain appears as ambient free subharmonic $\hat{\xi}_f$ in solution (3.5).

Equation (3.4) may be rewritten as

$$\hat{\xi}_g(x) = \int_a^b \hat{f}(y)\, G(y, y) \left[\frac{G(x, y)}{G(y, y)} \right] \mathrm{d}y. \qquad (3.6)$$

The initial complex amplitude of each emitted subharmonic generated per unit distance is $\hat{f}(y)G(y, y)$, whose spatial variation from y to x is described by $G(x, y)/G(y, y)$

967 A37-8

(figure 2). Accordingly, $\hat{f}(y)G(y, y)$ is defined as the source field of the group-induced subharmonic $\hat{\sigma}(y)$, i.e.

$$\hat{\sigma}(y) = \hat{f}(y)\, G(y, y).$$ (3.7)

Let $\hat{\xi}_h^+(x)$ and $\hat{\xi}_h^-(x)$ be the linearly independent homogeneous solutions of (2.16) that describe the downwave- and upwave-propagating free subharmonics, respectively. The Green's function that satisfies (3.1) can be constructed using two distinct linear combinations of $\hat{\xi}_h^+(x)$ and $\hat{\xi}_h^-(x)$ (see Ince 1956, p. 257). Assuming open boundaries at both $x = a$ and $x = b$, we seek a solution of $G(x, y)$ that satisfies the following boundary condition:

$$\frac{G(b, y)}{G(y, y)} = \frac{\hat{\xi}_h^+(b)}{\hat{\xi}_h^+(y)}, \qquad \frac{G(a, y)}{G(y, y)} = \frac{\hat{\xi}_h^-(a)}{\hat{\xi}_h^-(y)},$$ (3.8a,b)

which physically indicates that the local response generated at source location y arrives at boundary $x = a$ and $x = b$ as an upwave- and downwave-propagating free wave so that the spatial evolution of its complex amplitude is described by $\hat{\xi}_h^+$ or $\hat{\xi}_h^-$.

The solution for the governing equation (3.1) and the boundary condition (3.8a,b) is given by

$$G(x, y) = \begin{cases} G(y, y)\, \dfrac{\hat{\xi}_h^+(x)}{\hat{\xi}_h^+(y)}, & \text{for } x > y, \\[4mm] G(y, y)\, \dfrac{\hat{\xi}_h^-(x)}{\hat{\xi}_h^-(y)}, & \text{for } x < y, \end{cases}$$ (3.9)

with

$$G(y, y) = \left. \frac{\hat{\xi}_h^+ \hat{\xi}_h^-}{\hat{\xi}_h^- \dfrac{\mathrm{d}}{\mathrm{d}x}\hat{\xi}_h^+ - \hat{\xi}_h^+ \dfrac{\mathrm{d}}{\mathrm{d}x}\hat{\xi}_h^-} \right|_{x=y},$$ (3.10)

where the denominator of (3.10) is the Wronskian of $\hat{\xi}_h^-$ and $\hat{\xi}_h^+$, and it is non-zero owing to the linear independence between $\hat{\xi}_h^+$ and $\hat{\xi}_h^-$.

In (3.9), the Green's function at the source point $x = y$, $G(y, y)$, represents the initial complex amplitude of the subharmonic generated by the local unit point forcing, while the factor $\hat{\xi}_h^\pm(x)/\hat{\xi}_h^\pm(y) = G(x, y)/G(y, y)$ describes the relative changes in amplitude and phase of $G(x, y)$ from $x = y$ to $x = x$.

Substituting (3.9) into (3.6), and recalling the definition of the source field $\hat{\sigma}(y)$ (3.7), yields

$$\hat{\xi}_g(x) = \hat{\xi}_g^+(x) + \hat{\xi}_g^-(x),$$ (3.11)

where

$$\hat{\xi}_g^+(x) = \int_a^x \hat{\sigma}(y)\, \frac{\hat{\xi}_h^+(x)}{\hat{\xi}_h^+(y)}\, \mathrm{d}y, \qquad \hat{\xi}_g^-(x) = \int_x^b \hat{\sigma}(y)\, \frac{\hat{\xi}_h^-(x)}{\hat{\xi}_h^-(y)}\, \mathrm{d}y.$$ (3.12a,b)

The superscripts $+$ and $-$ denote the two components that form due to the downwave- and upwave-propagating free subharmonics being generated on the upwave and downwave sides of x, respectively.

Given the complex amplitudes of the ambient downwave- and upwave-propagating subharmonics at the boundary, i.e. $\hat{\xi}_f^+(a)$ and $\hat{\xi}_f^-(b)$, the ambient free subharmonic in the domain $a < x < b$ can be expressed as

$$\hat{\xi}_f(x) = \hat{\xi}_f^+(x) + \hat{\xi}_f^-(x), \tag{3.13}$$

where

$$\hat{\xi}_f^+(x) = \hat{\xi}_f^+(a) \frac{\hat{\xi}_h^+(x)}{\hat{\xi}_h^+(a)}, \quad \hat{\xi}_f^-(x) = \hat{\xi}_f^-(b) \frac{\hat{\xi}_h^-(x)}{\hat{\xi}_h^-(b)} \tag{3.14a,b}$$

describe the downwave- and upwave-propagating components, respectively. Note that $\hat{\xi}_f^\pm(x)$ differs from $\hat{\xi}_h^\pm(x)$ in that the former's boundary values vary with the boundary locations in the manner of a group-induced subharmonic instead of a free subharmonic, in order to incorporate the contribution of the source field in the incremental domain due to changing boundary locations. This is later demonstrated by the relationship between $\hat{\xi}_f^-(a)$ and $\hat{\xi}_f^-(b)$ in (3.17).

Substituting (3.11)–(3.14a,b) into (3.5) yields

$$\hat{\xi}(x) = \int_a^x \hat{\sigma}(y) \frac{\hat{\xi}_h^+(x)}{\hat{\xi}_h^+(y)} \, dy + \hat{\xi}_f^+(a) \frac{\hat{\xi}_h^+(x)}{\hat{\xi}_h^+(a)} + \int_x^b \hat{\sigma}(y) \frac{\hat{\xi}_h^-(x)}{\hat{\xi}_h^-(y)} \, dy + \hat{\xi}_f^-(b) \frac{\hat{\xi}_h^-(x)}{\hat{\xi}_h^-(b)}. \tag{3.15}$$

Equation (3.15) is the general form of the solution to (2.16), and its exact form depends on the expression of the wave radiation stress field and homogeneous solution. However, the solution in the form of (3.15) requires the information at two boundaries on both sides of x. To facilitate its practical applications, (3.15) can be rewritten as a solution with only one boundary for integration retained:

$$
\begin{aligned}
\hat{\xi}(x) &= \int_a^x \hat{\sigma}(y) \frac{\hat{\xi}_h^+(x)}{\hat{\xi}_h^+(y)} \, dy + \hat{\xi}_f^+(a) \frac{\hat{\xi}_h^+(x)}{\hat{\xi}_h^+(a)} \\
&\quad + \int_x^a \hat{\sigma}(y) \frac{\hat{\xi}_h^-(x)}{\hat{\xi}_h^-(y)} \, dy + \int_a^b \hat{\sigma}(y) \frac{\hat{\xi}_h^-(x)}{\hat{\xi}_h^-(y)} \, dy + \hat{\xi}_f^-(b) \frac{\hat{\xi}_h^-(x)}{\hat{\xi}_h^-(b)} \\
&= \hat{\xi}_f^+(a) \frac{\hat{\xi}_h^+(x)}{\hat{\xi}_h^+(a)} + \hat{\xi}_f^-(a) \frac{\hat{\xi}_h^-(x)}{\hat{\xi}_h^-(a)} + \int_a^x \hat{\sigma}(y) \left[\frac{\hat{\xi}_h^+(x)}{\hat{\xi}_h^+(y)} - \frac{\hat{\xi}_h^-(x)}{\hat{\xi}_h^-(y)} \right] dy, \tag{3.16}
\end{aligned}
$$

where

$$\hat{\xi}_f^-(a) = \hat{\xi}_f^-(b) \frac{\hat{\xi}_h^-(a)}{\hat{\xi}_h^-(b)} + \int_a^b \hat{\sigma}(y) \frac{\hat{\xi}_h^-(a)}{\hat{\xi}_h^-(y)} \, dy \tag{3.17}$$

is the complex amplitude of upwave-propagating free wave at $x = a$, which includes the contributions of free waves entering the region through the right-hand boundary $x = b$ and those generated due to the group forcing in the region $a < x < b$. The solution in the form of (3.16) is more computationally feasible than (3.15) and is used for the calculation in figure 6, but the former is physically not as intuitive as the latter because the effect of group forcing on the upwave-propagating components is manifested by deducting the contribution of sources along integral path from the overall contributions of sources.
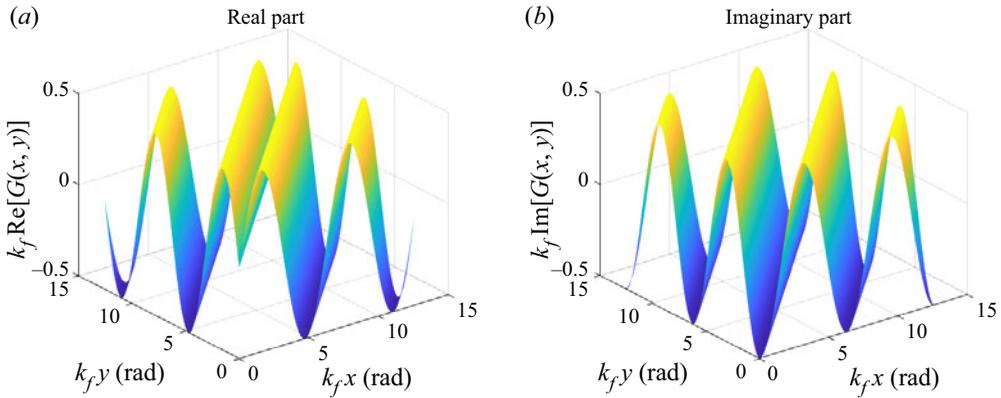
967 A37-10

Figure 3. (*a*) Real and (*b*) imaginary parts of the normalised Green's function for a flat bottom (3.21).

3.2. *Flat bottom*

Over a flat bottom, the governing equation (2.16) reduces to

$$\frac{d^2\hat{\xi}}{dx^2} + k_f^2\hat{\xi} = \hat{f}, \tag{3.18}$$

where the forcing term $\hat{f}$ is given by (3.2). According to (2.10)–(2.11), over a flat bottom $\hat{f}$ may be rewritten as

$$\hat{f}(x) = \frac{k_g^2\hat{S}(x)}{\rho gh} = \frac{k_g^2\hat{S}(a)}{\rho gh}e^{ik_g(x-a)} = \hat{f}(0)\,e^{ik_gx}, \tag{3.19}$$

which is in phase with the wave group. In addition, over a flat bottom, the homogeneous solutions to the governing equation (2.16) and thus the local response to unit point forcing described in equation (3.10) are given by

$$\hat{\xi}_h^\pm(x) = C^\pm e^{\pm ik_fx}, \quad G(y,y) = \frac{1}{2ik_f}, \tag{3.20a,b}$$

where $C^\pm$ is a non-zero constant.

Substituting (3.20*a,b*) into (3.9), we derive the Green's function for a flat bottom:

$$G(x,y) = \frac{1}{2ik_f}e^{ik_f|x-y|}, \tag{3.21}$$

where the variation of $G(x,y)$ with source location y and response location x is shown in figure 3. For a point unit forcing at $x = y$ described by $\delta_{Dirac}(x-y)e^{-i\omega_g t}$, the modulus and phase angle of $G(x,y)$ are the amplitude and phase lag with respect to the forcing of the subharmonic at x. The gradient of the real part of $G(x,y)$ is not continuous as the right-hand side of (3.1*c*) is real.

Substituting (3.19) and (3.20*b*) into the source field $\hat{\sigma}(y) = \hat{f}(y)G(y,y)$, we have

$$\hat{\sigma}(y) = \frac{\hat{f}(0)}{2ik_f}e^{ik_gy} = \frac{k_g^2}{2ik_f}\frac{\hat{S}(a)}{\rho gh}e^{ik_g(y-a)}, \tag{3.22}$$

which is spatially uniform in amplitude and leads the wave group by $\pi/2$ in phase as $\hat{S}(a)e^{ik_g(y-a)}$ is in phase with the wave group according to (2.10) and the phase of the

967 A37-11

complex factor i^{-1} is $-\pi/2$. Equation (3.22) indicates that each free subharmonic emitted from the source field has the same amplitude and is initially in quadrature with the wave group.

Substituting (3.20a) into (3.11)–(3.12a,b) yields the solution for $\hat{\xi}_g$:

$$\hat{\xi}_g(x) = \int_a^b \hat{\sigma}(y) \mathrm{e}^{\mathrm{i}k_f|x-y|}\,\mathrm{d}y. \tag{3.23a}$$

Invoking (3.22) further yields the expressions

$$\hat{\xi}_g(x) = \frac{\hat{f}(0)}{2\mathrm{i}k_f} \int_a^b \mathrm{e}^{\mathrm{i}(k_g y + k_f|x-y|)}\,\mathrm{d}y$$

$$= \frac{k_g^2}{2\mathrm{i}k_f} \frac{\hat{S}(a)}{\rho g h} \mathrm{e}^{-\mathrm{i}k_g a} \int_a^b \mathrm{e}^{\mathrm{i}(k_g y + k_f|x-y|)}\,\mathrm{d}y. \tag{3.23b}$$

Taking the integral in (3.23b) over the upwave side of x ($a < y < x$) yields the solution for $\hat{\xi}_g^+$ as defined in (3.12a):

$$\hat{\xi}_g^+(x) = \frac{k_g^2}{2\mathrm{i}k_f} \frac{\hat{S}(a)}{\rho g h} \mathrm{e}^{-\mathrm{i}k_g a} \int_a^x \mathrm{e}^{\mathrm{i}[k_g y + k_f(x-y)]}\,\mathrm{d}y$$

$$= \frac{k_g^2}{2\mathrm{i}k_f} \frac{\hat{S}(a)}{\rho g h} \mathrm{e}^{\mathrm{i}(k_f x - k_g a)} \int_a^x \mathrm{e}^{\mathrm{i}(k_g - k_f)y}\,\mathrm{d}y$$

$$= -\frac{k_g^2}{2k_f} \frac{\hat{S}(x) - \hat{S}(a)\mathrm{e}^{\mathrm{i}k_f(x-a)}}{\rho g h(k_g - k_f)}, \tag{3.24}$$

where the relationship $\hat{S}(x) = \hat{S}(a)\mathrm{e}^{\mathrm{i}k_g(x-a)}$ is used. Similarly, the solution for $\hat{\xi}_g^-$ is derived by integrating over the downwave side $x < y < b$ as

$$\hat{\xi}_g^-(x) = \frac{k_g^2}{2k_f} \frac{\hat{S}(x) - \hat{S}(b)\mathrm{e}^{-\mathrm{i}k_f(x-b)}}{\rho g h(k_g + k_f)}, \tag{3.25}$$

where the relationship $\hat{S}(x) = \hat{S}(b)\mathrm{e}^{\mathrm{i}k_g(x-b)}$ is used. Let $\hat{\xi}_b^+$ and $\hat{\xi}_b^-$ be the corresponding components bound to $\hat{S}(x)$ and therefore wave group in (3.24) and (3.25), i.e.

$$\hat{\xi}_b^\pm(x) = \mp \frac{k_g^2}{2k_f(k_g \mp k_f)} \frac{\hat{S}(x)}{\rho g h}. \tag{3.26}$$

Equations (3.24) and (3.25) can be rewritten as

$$\left.\begin{array}{l}
\hat{\xi}_g^+(x) = \hat{\xi}_b^+(x) - \hat{\xi}_b^+(a)\,\mathrm{e}^{\mathrm{i}k_f(x-a)}, \\[2mm]
\hat{\xi}_g^-(x) = \hat{\xi}_b^-(x) - \hat{\xi}_b^-(b)\,\mathrm{e}^{-\mathrm{i}k_f(x-b)}.
\end{array}\right\} \tag{3.27}$$

3.2.1. *Intermediate water*

In intermediate water, $c_g < \sqrt{gh}$ and $k_g > k_f$. Figure 4(a) shows the spatial variation of the phase of all subharmonics emitted for the source location y and the observation position x, as described by $\exp[\mathrm{i}(k_g y + k_f|x-y|)]$ (the integrand in (3.23b)). On the one hand, at each
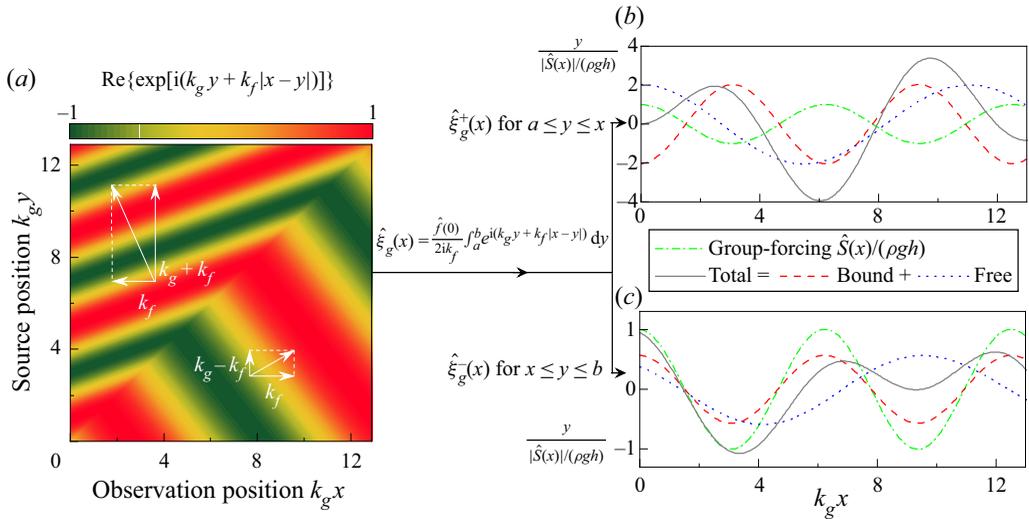
967 A37-12

Figure 4. Diagram of the emission, propagation and interference of subharmonics generated from the source field $\hat{\sigma}(y) = \hat{f}(y)G(y, y)$ due to group forcing of bichromatic waves over a flat bottom in intermediate depth ($k_g > k_f$, where $k_g = \omega_g/c_g$ and $k_f = \omega_g/\sqrt{gh}$ are the wavenumbers of wave group and free subharmonic propagating as shallow-water wave, respectively). Here $\hat{f}$ is the forcing term and $G(y, y)$ is the Green's function at $x = y$. (a) Term $\exp[i(k_g y + k_f|x - y|)]$ gives the spatial variation of product of source field and Green's function as shown in (3.23), which in turn describe the spatial variation of the free subharmonic with its source position y and observation position x. The vertical and horizontal white arrows denote the wavenumber of each emitted subharmonic component on the source and observation position, respectively. (b) The y axis denotes the real part of the superposed downwave-propagating subharmonic ($\hat{\xi}_g^+$, (3.24)), showing the surface elevation snapshot for $t = 0$. (c) Similar to (b) but for the upwave component ($\hat{\xi}_g^-$, (3.25)).

given y, the horizontal slice of figure 4(a) describes the phase change of the upwave- and downwave-propagating subharmonics emitted from $x = y$, resembling the picture shown in figure 2. On the other hand, at each given x, the vertical slice of figure 4(a) describes the phase variation with the source location y of all subharmonics arriving at x. Figure 4(b,c) shows that the superposition of all free subharmonics can be further decomposed into a subharmonic bound to the wave group and a free subharmonic which are respectively described by the first and second terms on the right-hand side of (3.27).

The emergence of a bound subharmonic from the superposition of all free subharmonics is essentially the consequence of wave-group-modulated emission of each free subharmonic through the source field bound to the wave group, which does not conflict with the interpretation of the group-induced subharmonic as the superposition of free subharmonics. More specifically, the modulated emission means the phase of the source field by (3.22) varies with space as $k_g y$ due to direct modulation of group forcing, indicating that free subharmonics with the same initial phase are generated at equidistant locations separated by $2\pi/k_g$, i.e. one wave-group length. Consequently, a *de facto* waveform with the same wavelength as the wave group forms and appears phase locked to the wave group, i.e. so-called bound subharmonic in previous studies. Similarly, in (3.27), the superposition of all the upwave-propagating free subharmonics leads to a downwave-propagating bound subharmonic. However, for an observer at a fixed observation position, the bound subharmonic does not exist because there is no space for the aforementioned superposition of the emitted free subharmonics to occur, which
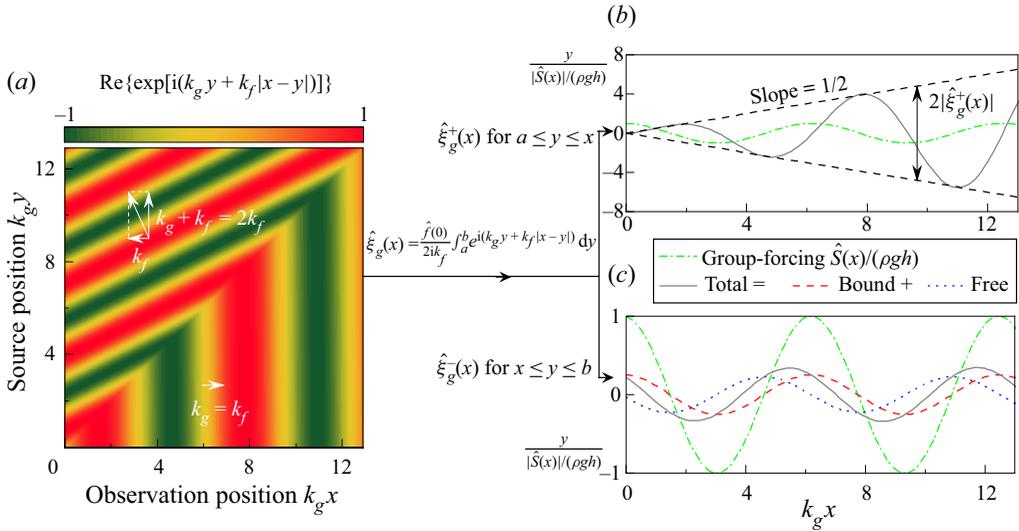
Figure 5. Same as figure 4, but for shallow water where $c_g = \sqrt{gh}$ and $k_g = k_f$, where $k_g = \omega_g/c_g$ and $k_f = \omega_g/\sqrt{gh}$ are wavenumbers of wave group and free subharmonic propagating as shallow-water wave, respectively. The vertical and horizontal white arrows denote the wavenumber of the emitted subharmonic component on the source and observation position, respectively. Values of the group-forcing lines in (*b*,*c*) are the same for reference.

mathematically corresponds to an integral interval of zero length in (3.4), and only the free subharmonics arriving from elsewhere will be observed.

Interestingly, (3.26) shows that $\hat{\xi}_b^+(x)$ and $\hat{\xi}_b^-(x)$ are respectively in antiphase and phase with the wave groups, and $|\hat{\xi}_b^+|$ is $(k_g + k_f)/(k_g - k_f)$ times larger than $|\hat{\xi}_b^-|$. Thus, the expression for the total bound subharmonics $\hat{\xi}_b = \hat{\xi}_b^+ + \hat{\xi}_b^-$ is given by

$$\hat{\xi}_b(x) = \left[\frac{1}{(k_g + k_f)} - \frac{1}{(k_g - k_f)} \right] \frac{k_g^2}{2k_f} \frac{\hat{S}(x)}{\rho gh} = -\frac{k_g^2}{k_g^2 - k_f^2} \frac{\hat{S}(x)}{\rho gh}, \tag{3.28}$$

which is in antiphase with the group forcing. Equation (3.28) is the same as the LHS62 solution:

$$\hat{\xi}_{LHS62}(x) = -\frac{\hat{S}(x)}{\rho(gh - c_g^2)}. \tag{3.29}$$

3.2.2. *Shallow water*
In shallow water, $c_g \to \sqrt{gh}$ and $k_g \to k_f$, the diagram in figure 4 changes to that in figure 5 and the emitted downwave-propagating subharmonics are now in phase with each other. This is because according to (3.12*a*) the phase of the downwave-propagating subharmonic emitted from y is $\arg[\hat{\sigma}(y)\hat{\xi}_h^+(x)/\hat{\xi}_h^+(y)] \propto (k_g - k_f)y + k_f x$, which becomes independent of its source position y as $k_g \to k_f$, indicating that all downwave-propagating subharmonics interfere with each other constructively. In addition, because the initial amplitudes of all the downwave subharmonics are the same, the superposed amplitude of $|\hat{\xi}_g^+|$ increases proportionally with the number of forcing pulses, which in turn increases linearly with travel distance $k_g x$.
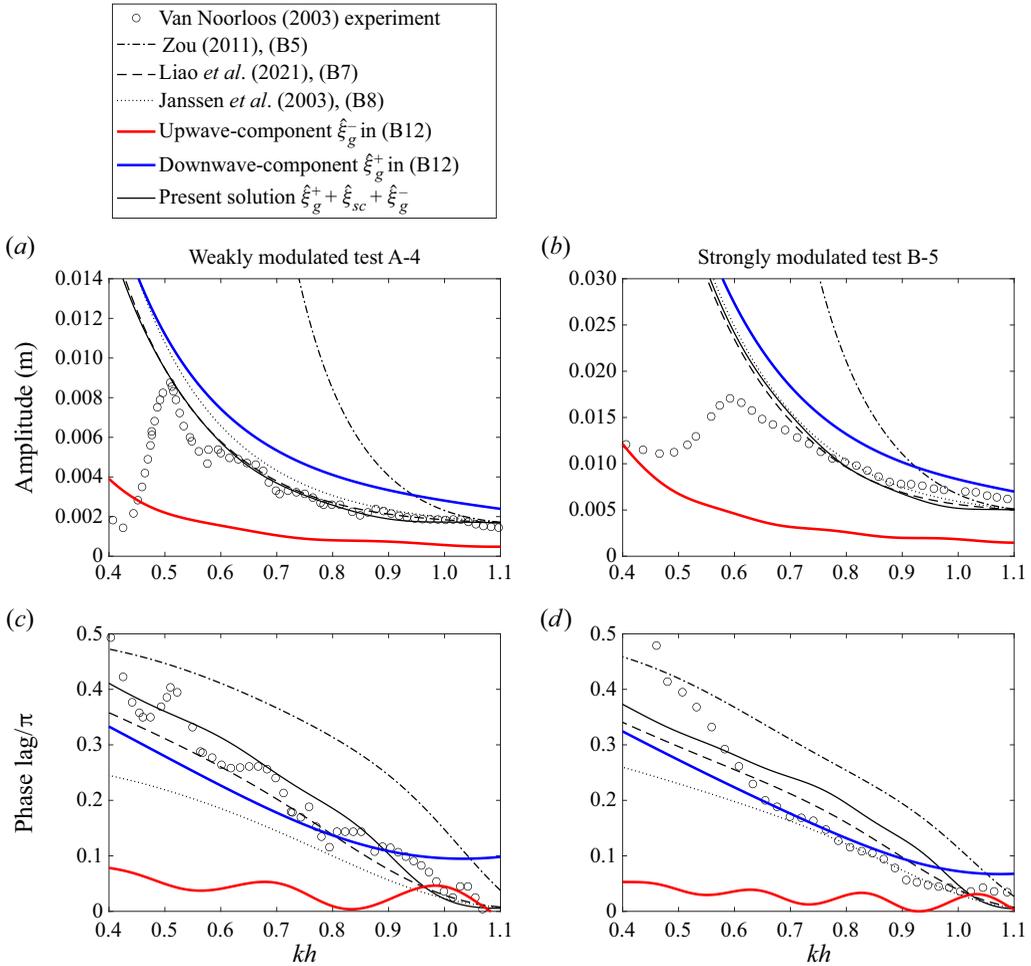
967 A37-14

Figure 6. Amplitude (a,b) and phase (c,d) of the complex amplitude $\hat{\xi}(x)$ of the subharmonic surface elevation $\tilde{\xi}(x,t)$ forced by bichromatic wave groups normally incident over a plane sloping bottom. Wave conditions and topography of tests A-4 (a,c) and B-5 (b,d) of the flume experiment of Van Noorloos (2003). Laboratory measurements (circles), the off-resonant solution of Zou (2011) ((B5), black dash-dotted lines), the near-resonance solution of Liao *et al.* (2021) ((B7), black dashed lines), Janssen *et al.* (2003) ((B8), black dotted lines), the present solution $\hat{\xi} = \hat{\xi}_g^+ + \hat{\xi}_{sc} + \hat{\xi}_g^-$ where $\hat{\xi}_{sc}$ denotes the downwave free subharmonic generated due to scattering at the slope toe ((B11), black solid lines) and its downwave- and upwave-propagating group-induced subharmonic components, $\hat{\xi}_g^+$ (blue lines) and $\hat{\xi}_g^-$ (red lines) in (B12). Phase is the phase lag with respect to wave groups plus π. Note that in (b), the phase of the upwave component $\hat{\xi}_g^-$ was manually shifted by π for plotting purposes.

This result can also be derived by taking the limit $k_g \rightarrow k_f$ for $\hat{\xi}_g^+$ in (3.27). From (2.10)–(2.11) we have $\hat{S}(x) = \hat{S}(a)e^{ik_g(x-a)}$ over a flat bottom. Substituting this for $\hat{S}(x)$ in (3.26) and subsequently (3.26) into (3.27) for $\hat{\xi}_g^+$ and then taking the limit $k_g \rightarrow k_f$, we have

$$\lim_{k_g \rightarrow k_f} \hat{\xi}_g^+(x) = \lim_{k_g \rightarrow k_f} -\frac{k_g^2}{2k_f}\frac{\hat{S}(a)}{\rho gh}\frac{e^{ik_g(x-a)} - e^{ik_f(x-a)}}{k_g - k_f} = \frac{k_f(x-a)\hat{S}(x)}{2i\rho gh}. \tag{3.30}$$

Thus, $|\hat{\xi}_g^+|$ is proportional to the travel distance $k_g(x-a)$. Equation (3.30) also shows that the downwave group-induced subharmonic leads the group forcing by $\pi/2$ because of the complex factor i^{-1}, since each emitted downwave-propagating subharmonic is initially ahead of the group forcing by $\pi/2$ according to (3.22).

Remarkably, in (3.30), the bound subharmonic cannot be distinguished from the free mode as in (3.27); hence, it is only meaningful to describe the superposed downwave-propagating group-induced subharmonic as a whole. This phenomenon indicates that $\hat{\xi}_b^+$ is released when the system is in full resonance. To some extent, it is consistent with the viewpoint of Baldock (2012) that the bound subharmonic is released in shallow water with and without wave breaking. Nevertheless, the resonance only occurs in the propagating direction of group forcing, not in the upwave-propagating direction. Thereby, the present result partially differs from that of Baldock (2012) in that the bound subharmonic component $\hat{\xi}_b^-$ still exists in shallow water. This can be found by taking the limit $k_g \to k_f$ for $\hat{\xi}_b^-$ in (3.26):

$$\lim_{k_g \to k_f} \hat{\xi}_b^- (x) = \lim_{k_g \to k_f} \frac{k_g^2}{2k_f \left(k_g + k_f\right)} \frac{\hat{S}(x)}{\rho g h} = \frac{\hat{S}(x)}{4\rho g h}. \tag{3.31}$$

When the resonance occurs, $|\hat{\xi}_g^+|$ far exceeds $|\hat{\xi}_b^-|$ after a certain distance (figure 5b,c), hence dominating $\hat{\xi}_g$.

3.3. *Uneven bottom*

Over an uneven bottom, assuming a mild bottom slope, i.e. $|\beta| = |h_x/(k_g h)| < |h_x/(k_f h)| \ll 1$ and $h_{xx}/(k_g h) = O(\beta^2)$, substituting (2.10) into the forcing field (3.2) yields

$$\hat{f}(x) = \frac{k_g^2 \left|\hat{S}\right|}{\rho g h} \left(-\frac{1}{k_g^2 \left|\hat{S}\right|} \frac{d^2 \left|\hat{S}\right|}{d x^2} - \frac{2i}{k_g \left|\hat{S}\right|} \frac{d \left|\hat{S}\right|}{d x} - \frac{i}{k_g^2} \frac{dk_g}{d x} + 1 \right) e^{i \int^x k_g \, d x'}. \tag{3.32}$$

Following Zou (2011), (3.32) can be decomposed into $\hat{f}_M$ at leading order, which is the forcing field for a flat bottom in (3.19), $\hat{f}_S$ induced by bottom slope and $\hat{f}_r$ due to higher-order bottom gradient h_x^2 and h_{xx}, i.e.

$$\hat{f} = \hat{f}_M + \hat{f}_S + \hat{f}_r, \tag{3.33}$$

where

$$\left.\begin{array}{l} \hat{f}_M = \dfrac{k_g^2 \left|\hat{S}\right|}{\rho g h} \exp \left(i \int^x k_g \, d x' \right), \\[4mm] \hat{f}_S = \hat{f}_M \left(-\dfrac{2i}{k_g \left|\hat{S}\right|} \dfrac{d \left|\hat{S}\right|}{d x} - \dfrac{i}{k_g^2} \dfrac{dk_g}{d x} \right) = \hat{f}_M O \left(\beta\right), \\[4mm] \hat{f}_r = \hat{f}_M \left(-\dfrac{1}{k_g^2 \left|\hat{S}\right|} \dfrac{d^2 \left|\hat{S}\right|}{d x^2} \right) = \hat{f}_M O \left(\beta^2\right), \end{array}\right\} \tag{3.34}$$

which is the same as the forcing field in Zou (2011).

967 A37-16

The homogeneous solution in this case can be obtained by the perturbation method utilising the small parameter of $h_x/(k_f h)$. At leading order of $O(1)$, the homogeneous solution is given by (cf. Zou 2011, equation (3.9c))

$$\hat{\xi}_h^{\pm}(x) = C^{\pm} h^{-0.25}(x) \exp\left(i \int^x \pm k_f \, dx'\right)\left[1 + O\left(\beta \frac{k_g}{k_f}\right)\right], \qquad (3.35)$$

which is substituted into (3.10) to yield

$$G(y, y) = \frac{1}{2i k_f(y)}\left[1 + O\left(\beta \frac{k_g}{k_f}\right)\right]. \qquad (3.36)$$

Linearised to the first order of bottom slope, the forcing field (3.33) becomes

$$\hat{f}_L = \hat{f}_M + \hat{f}_S = \frac{k_g^2 \left|\hat{S}\right|}{\rho g h}\left(1 - \frac{2i}{k_g \left|\hat{S}\right|}\frac{d\left|\hat{S}\right|}{dx} - \frac{i}{k_g^2}\frac{dk_g}{dx}\right)\exp\left(i \int^x k_g \, dx'\right), \qquad (3.37)$$

which together with (3.36) are substituted into (3.7) to yield the expression for the source field $\hat{\sigma}(y)$:

$$\hat{\sigma}(y) = \frac{k_g^2 \left|\hat{S}\right|}{2i k_f \rho g h}\left(1 - \frac{2i}{k_g \left|\hat{S}\right|}\frac{d\left|\hat{S}\right|}{dx} - \frac{i}{k_g^2}\frac{dk_g}{dx}\right)\exp\left(i \int^y k_g \, dx'\right)\left[1 + O\left(\beta \frac{k_g}{k_f}\right)\right]. \qquad (3.38)$$

Substituting (3.38) and (3.35) into (3.12a,b) yields

$$\left.\begin{aligned}
\hat{\xi}_g^+(x) &= \int_a^x \frac{\hat{f}_L(y)}{2i k_f(y)}\left[\frac{h(x)}{h(y)}\right]^{-0.25}\exp\left(i \int_y^x k_f \, dx'\right)\left[1 + O\left(\beta \frac{k_g}{k_f}\right)\right] dy, \\
\hat{\xi}_g^-(x) &= \int_x^b \frac{\hat{f}_L(y)}{2i k_f(y)}\left[\frac{h(x)}{h(y)}\right]^{-0.25}\exp\left(-i \int_y^x k_f \, dx'\right)\left[1 + O\left(\beta \frac{k_g}{k_f}\right)\right] dy.
\end{aligned}\right\} \qquad (3.39)$$

The phase dependence of the integrand in (3.39) on source location y determines the interference among all free components generated from different sources arriving at observation point x. At leading order, $\hat{f}_L(y)$ in (3.37) is in phase with the wave group and hence its phase varies with y as $\int^y k_g \, dx'$. Therefore, in (3.39) the phase of each component of $\hat{\xi}_g^{\pm}$ mainly varies with y as $\int^y k_g \pm k_f \, dx'$, which largely determines the relative magnitude between $\hat{\xi}_g^+$ and $\hat{\xi}_g^-$ as discussed in detail in Appendix C.

3.3.1. *Shallow water*

In shallow water, according to (3.26)–(3.27), as $k_g \to k_f$ and the resonance is intensified, $\hat{\xi}_g^+$ becomes the predominant part of the group-induced subharmonic, i.e. $\hat{\xi}_g \approx \hat{\xi}_g^+$.

Without wave breaking, given the shallow-water approximations of $c_g \approx c \approx \sqrt{gh}$ and $k_g = \omega_g/c_g \approx \omega_g/\sqrt{gh}$, (2.11) indicates $|\hat{S}(x)| = |\hat{S}(a)|\sqrt{h(a)/h(x)}$. Hence the spatial

evolution of $\hat{S}$ described by the energy conservation (2.10)–(2.11) becomes

$$\hat{S}(x) = \hat{S}(a) \left[\frac{h(x)}{h(a)} \right]^{-0.5} \exp\left(i \int_a^x \frac{\omega_g}{\sqrt{gh}} \, dx' \right). \tag{3.40}$$

Substituting (3.40) into the forcing term (3.32) yields

$$\hat{f}(x) = \frac{\omega_g^2}{gh(x)} \frac{\hat{S}(a)}{\rho gh(x)} \left[\frac{h(x)}{h(a)} \right]^{-0.5} \exp\left(i \int_a^x \frac{\omega_g}{\sqrt{gh}} \, dx' \right) [1 + O(\beta)] \tag{3.41}$$

at leading order.

Substituting (3.41) into the solution for $\hat{\xi}_g^+$ in (3.39) yields

$$\hat{\xi}_g^+(x) = \frac{\omega_g \hat{S}(a)}{2i\rho g^{1.5}} \left[\frac{h(x)}{h(a)} \right]^{-0.5} \left[h^{0.25}(x) \int_a^x h(y)^{-1.75} \, dy \right] \exp\left(i \int_a^x \frac{\omega_g}{\sqrt{gh}} \, dx' \right) \tag{3.42}$$

at leading order, which is dependent on the bottom profile. The amplitude of $\hat{\xi}_g^+$ in (3.42) is proportional to $\int_a^x h(y)^{-1.75} \, dy$, which in turn is proportional to the horizontal length of the bottom profile between a and x. More specifically, suppose that the topography is horizontally stretched by a factor; considering the integrand in $\int_a^x h(y)^{-1.75} \, dy$ is only a function of depth, the integral covering the same bottom profile would also be enlarged by the same factor, and so is the amplitude of $\hat{\xi}_g^+$. This is essentially ascribed to the same accumulative constructive interference process of the downwave-propagating subharmonics demonstrated in figure 5, which causes the subharmonic amplitude to increase linearly with travel distance. This finding is consistent with the semi-analytical result of Liao *et al.* (2021) that the amplitude of a group-induced subharmonic over the front slope of a shoal increases with the travel distance.

Over a uniform slope ($h_x = \text{const.}$), (3.42) reduces to

$$\hat{\xi}_g^+(x) = \frac{2i}{3} \frac{\omega_g}{h_x} \sqrt{\frac{h(a)}{g}} \left[\frac{h(a)}{h(x)} - \left(\frac{h(a)}{h(x)} \right)^{0.25} \right] \frac{\hat{S}(a)}{\rho gh(a)} \exp\left(i \int_a^x \frac{\omega_g}{\sqrt{gh}} \, dx' \right). \tag{3.43}$$

Invoking (3.40) reduces (3.43) further to

$$\hat{\xi}_g^+(x) = \frac{2i}{3} \frac{\omega_g}{h_x} \sqrt{\frac{h(x)}{g}} \frac{\hat{S}(x)}{\rho gh(x)} - \frac{2i}{3} \frac{\omega_g}{h_x} \sqrt{\frac{h(a)}{g}} \frac{\hat{S}(a)}{\rho gh(a)} \left[\frac{h(x)}{h(a)} \right]^{-0.25} \exp\left(i \int_a^x \frac{\omega_g}{\sqrt{gh}} \, dx' \right), \tag{3.44}$$

where the first term is consistent with the shallow-water limit of the near-resonant solution by equation (20) of Liao *et al.* (2021) and the second term represents a free subharmonic. The second term appears because only the forcing inside the finite region a to x is considered; therefore, $\hat{\xi}_g^+(a) = 0$ has to be satisfied at the boundary $x = a$. Equation (3.44) indicates that the amplitude of group-induced subharmonic is inversely proportional to the bottom slope in shallow water, which is due to the increase of group-induced subharmonic amplitude linearly with travel distance. This result provides a theoretical explanation for the well-known decrease of shoaling rate of group-induced subharmonic with the relative bottom slope (e.g. Battjes *et al.* 2004; Van Dongeren *et al.* 2007; De Bakker, Tissier & Ruessink 2016; Zhang, Toorman & Monbaliu 2020). The dependence of subharmonic amplitude on the travel distance of wave groups corroborates the historical effect of spatial

967 A37-18

evolution of wave groups in the region of shallow water on the subharmonic amplitude in the subsequent region as previously studied by Li *et al.* (2020) and Liao *et al.* (2021). Apart from that, the present model indicates that the group-forcing field also affects the subharmonic on the upwave side because of the generation of those upwave-propagating subharmonics. The topographic effect on the group-induced subharmonics is examined in detail in Appendix D.

4. Comparisons of present and previous solutions

The present unified solution is shown to reduce to the existing solutions (Van Leeuwen 1992; Schäffer 1993; Janssen *et al.* 2003; Zou 2011; Contardo *et al.* 2021; Liao *et al.* 2021) in this section.

4.1. *Solution over a plane sloping beach*

The solution of the group-induced subharmonic over a plane sloping beach was obtained by Van Leeuwen (1992) and Schäffer (1993). For a plane sloping beach with $x = 0$ at the shoreline, $h = h_x x$, where $h_x < 0$ is a constant, the governing equation (2.16) can be rewritten with the new dependent variable

$$u = \frac{2\omega_g}{gh_x}\sqrt{gh} \tag{4.1}$$

as

$$u^2 \frac{\mathrm{d}^2\hat{\xi}}{\mathrm{d}u^2} + u\frac{\mathrm{d}\hat{\xi}}{\mathrm{d}u} + u^2\hat{\xi} = -\frac{4h}{\rho g h_x^2}\frac{\mathrm{d}^2\hat{S}}{\mathrm{d}x^2}, \tag{4.2}$$

whose homogeneous solutions are given by

$$\left.\begin{aligned}
\hat{\xi}_h^+(x) &= \mathrm{H}_0^{(2)}\left[u(x)\right] = \mathrm{J}_0\left[u(x)\right] - \mathrm{i}\mathrm{Y}_0\left[u(x)\right], \\
\hat{\xi}_h^-(x) &= \mathrm{H}_0^{(1)}\left[u(x)\right] = \mathrm{J}_0\left[u(x)\right] + \mathrm{i}\mathrm{Y}_0\left[u(x)\right],
\end{aligned}\right\} \tag{4.3}$$

where $\mathrm{H}_0^{(1)}$ and $\mathrm{H}_0^{(2)}$ are the first- and second-kind Hankel function of order zero and J_0 and Y_0 are the zeroth-order Bessel function of the first and second kind. Note that $\mathrm{H}_0^{(2)}$ instead of $\mathrm{H}_0^{(1)}$ becomes $\hat{\xi}_h^+(x)$ because as x increases the phase of $\hat{\xi}_h^+(x)$ must increase. The Wronskian of $\hat{\xi}_h^-$ and $\hat{\xi}_h^+$ in the denominator of (3.10) now becomes

$$\begin{aligned}
\hat{\xi}_h^-&(x)\frac{\mathrm{d}}{\mathrm{d}x}\hat{\xi}_h^+(x) - \hat{\xi}_h^+(x)\frac{\mathrm{d}}{\mathrm{d}x}\hat{\xi}_h^-(x) \\
&= \left[\mathrm{H}_0^{(1)}(u)\frac{\mathrm{d}}{\mathrm{d}u}\mathrm{H}_0^{(2)}(u) - \mathrm{H}_0^{(2)}(u)\frac{\mathrm{d}}{\mathrm{d}u}\mathrm{H}_0^{(1)}(u)\right]\frac{\mathrm{d}u}{\mathrm{d}x} \\
&= -\frac{4\mathrm{i}}{\pi u}\frac{\omega_g}{\sqrt{gh}} = -\frac{2\mathrm{i}}{\pi}\frac{h_x}{h}.
\end{aligned} \tag{4.4}$$

Substituting (3.2), (4.3) and (4.4) into (3.7) yields

$$\hat{\sigma}(y) = -\frac{\mathrm{i}\pi h}{2h_x}\frac{\mathrm{H}_0^{(1)}[u(y)]\mathrm{H}_0^{(2)}[u(y)]}{\rho g h}\frac{\mathrm{d}^2\hat{S}}{\mathrm{d}x^2}. \tag{4.5}$$

Substituting (4.3) and (4.5) into the solution (3.16) yields

$$\hat{\xi}(x) = H_0^{(1)}\left[u(x)\right]\left[\frac{\hat{\xi}_f^-(a)}{H_0^{(1)}\left[u(a)\right]} + \frac{i\pi}{2\rho g h_x}\int_a^x H_0^{(2)}[u(y)]\frac{\mathrm{d}^2\hat{S}}{\mathrm{d}x^2}\,\mathrm{d}y\right]$$
$$+ H_0^{(2)}\left[u(x)\right]\left[\frac{\hat{\xi}_f^+(a)}{H_0^{(2)}\left[u(a)\right]} - \frac{i\pi}{2\rho g h_x}\int_a^x H_0^{(1)}[u(y)]\frac{\mathrm{d}^2\hat{S}}{\mathrm{d}x^2}\,\mathrm{d}y\right], \qquad (4.6)$$

which is equivalent to the solution given by equation (4.16) in Schäffer (1993). Moreover, the non-homogeneous part of (4.6) can be easily converted to the solution given by equation (3.1.62) in Van Leeuwen (1992) using the definition of Hankel function in (4.3).

4.2. *Off-resonant solution for intermediate water*

Let $\mu = 1 - k_f^2/k_g^2$ measure the departure of the system from resonance (Janssen *et al.* 2003), which decreases from $O(1)$ in intermediate water to zero in shallow water, and let β/μ measure the resonance intensity of the system. The parameter regime of $\beta\mu^{-1} = O(\beta)$ in intermediate water and $\beta\mu^{-1} = O(1)$ are referred to as off- and near-resonance conditions, respectively, as per Janssen *et al.* (2003). Under off-resonant condition, Janssen *et al.* (2003), Zou (2011) and Liao *et al.* (2021) derived the analytical solution of subharmonic for uneven bottom using perturbation expansion with small parameter β. Accurate to order $O(\beta)$, their group-bounded subharmonic solutions are equivalent to each other:

$$\hat{\xi}_b = -\frac{\hat{S}}{\rho g h\mu}\left\{1 + \frac{i\beta}{\mu}\left[\left(\frac{2h}{|\hat{S}|}\frac{\mathrm{d}\left|\hat{S}\right|}{\mathrm{d}h} + \frac{h}{k_g}\frac{\mathrm{d}k_g}{\mathrm{d}h}\right)(1-\mu) - 1 - \frac{2h}{\mu}\frac{\mathrm{d}\mu}{\mathrm{d}h}\right] + O(\beta^2)\right\}. \tag{4.7}$$

For an uneven bottom in intermediate water, the solution (3.11) can be first transformed into (3.39). The phase factor of the integrand in (3.39) is $\exp(i\int^y k_g \pm k_f\,\mathrm{d}x')$ for $\hat{\xi}_g^\pm(x)$, and applying the integration by parts technique to (3.39) using this phase factor twice, and retaining the variable upper bound of the integral, yields

$$\hat{\xi}_b^\pm = \pm\frac{\hat{f}_L}{2ik_f}\left\{\frac{1}{i\left(k_g \mp k_f\right)} + \frac{1}{\left(k_g \mp k_f\right)^2}\left[\frac{h^{0.25}f_L}{k_f\left(k_g \mp k_f\right)}\right]^{-1}\frac{\mathrm{d}}{\mathrm{d}x}\left[\frac{h^{0.25}f_L}{k_f\left(k_g \mp k_f\right)}\right]\right\}$$
$$\times \left[1 + O\left(\beta\frac{k_g}{k_f}\right)\right], \tag{4.8}$$

where $f_L = \hat{f}_L|\hat{S}|\hat{S}^{-1} = (\hat{f}_M + \hat{f}_S)|\hat{S}|\hat{S}^{-1}$ is the linearised forcing term excluding the phase factor of wave group.

Substituting (3.37) and $\mu = 1 - k_f^2/k_g^2$ into (4.8), we have

$$\hat{\xi}_b^\pm(x) = \mp\frac{\hat{S}}{\rho g h\mu}\frac{k_g \pm k_f}{2k_f}\left[\begin{array}{l}\left(1 - \frac{2i}{k_g|\hat{S}|}\frac{\mathrm{d}|\hat{S}|}{\mathrm{d}x} - \frac{i}{k_g^2}\frac{\mathrm{d}k_g}{\mathrm{d}x}\right) - \frac{k_g \pm k_f}{ik_g^2\mu}\left(\frac{|\hat{S}|}{h^{0.25}\mu}\right)^{-1}\\ \times\frac{\mathrm{d}}{\mathrm{d}x}\left(\frac{|\hat{S}|}{h^{0.25}\mu}\right) - \frac{1}{ik_g^2\mu}\frac{\mathrm{d}}{\mathrm{d}x}\left(k_g \pm k_f\right) + O\left(\beta\frac{k_g}{k_f}\right)\end{array}\right]. \tag{4.9}$$

967 A37-20

Adding $\hat{\xi}_b^+$ and $\hat{\xi}_b^-$ in (4.9) yields

$$\hat{\xi}_b = \hat{\xi}_b^+ + \hat{\xi}_b^-$$
$$= -\frac{\hat{S}}{\rho g h \mu}\left\{1 + \frac{\mathrm{i}\beta}{\mu}\left[\left(\frac{2h}{\left|\hat{S}\right|}\frac{\mathrm{d}\left|\hat{S}\right|}{\mathrm{d}h} + \frac{h}{k_g}\frac{\mathrm{d}k_g}{\mathrm{d}h}\right)(1-\mu) - 1 - \frac{2h}{\mu}\frac{\mathrm{d}\mu}{\mathrm{d}h}\right] + O\left(\beta^2\right)\right\}, \tag{4.10}$$

which is the same as solution (4.7). Note that the relative error for $\hat{\xi}_b^{\pm}$ in (4.9) is of $O[h_x/(k_f h)]$, but the error for $\hat{\xi}_b$ in (4.10) is of $O(\beta^2)$ (see Appendix A for more details).

4.3. *Near-resonant solution for shallow water*

4.3.1. *Liao et al. (2021) solution*
In the case of near resonance in shallow water ($\beta\mu^{-1} = O(1)$), Liao *et al.* (2021) derived the following solution of group-induced subharmonic (cf. equation (19) therein):

$$\hat{\xi}_g(x) = -\frac{\mathrm{i}\hat{S}(x)}{2\rho g h(x)}\int_a^x \left|\frac{\hat{S}(y)}{\hat{S}(x)}\right|\sqrt{\frac{k_g(y)h(x)}{k_g(x)h(y)}}k_g(y)\exp\left(-\mathrm{i}\int_y^x \frac{\mu}{2}k_g\,\mathrm{d}x'\right)\mathrm{d}y\,[1 + O(\beta)]. \tag{4.11}$$

The relationship $\hat{S}(x)/|\hat{S}(x)| = \hat{S}(y)/|\hat{S}(y)|\exp(\mathrm{i}\int_y^x k_g\,\mathrm{d}x')$ could be derived from (2.10) and then substituted together with $\hat{f}_M$ in (3.34) into (4.11) to obtain

$$\hat{\xi}_g(x) = \int_a^x \frac{\hat{f}_M(y)}{2\mathrm{i}k_g(y)}\,[1 + O(\beta)]\sqrt{\frac{k_g(y)h(y)}{k_g(x)h(x)}}\exp\left(\mathrm{i}\int_y^x\left(1 - \frac{\mu}{2}\right)k_g\,\mathrm{d}x'\right)\mathrm{d}y. \tag{4.12}$$

In this condition, (3.26)–(3.27) indicate that $|\hat{\xi}_g^+|$ is greater than $|\hat{\xi}_g^-|$ by an order of factor $(k_g + k_f)/(k_g - k_f) = (1 + \sqrt{1-\mu})/(1 - \sqrt{1-\mu})$, which is of $O(\mu^{-1}) = O(\beta^{-1})$ for $\mu = O(\beta) \ll 1$ in shallow water. Besides, as shown in Appendix A, the error of (3.39) is now of $O(\beta)$ relative to leading order, and hence we aim to prove that the solution for $\hat{\xi}_g^+$ in (3.39) at leading order

$$\hat{\xi}_g(x) = \int_a^x \frac{\hat{f}_M(y)}{2\mathrm{i}k_f(y)}\,[1 + O(\beta)]\left[\frac{h(x)}{h(y)}\right]^{-0.25}\exp\left(\mathrm{i}\int_y^x k_f\,\mathrm{d}x'\right)\mathrm{d}y \tag{4.13}$$

is consistent with (4.12).

Because $k_f/k_g = \sqrt{1-\mu} = 1 + O(\beta)$ and $k_g - k_f = k_g(1 - \sqrt{1-\mu}) = k_g[\mu/2 + O(\beta^2)]$, hence $[1 - \mu/2 + O(\beta^2)]k_g = k_f$ and at leading order the integrands of (4.12) and (4.13) are consistent with each other and so are the two solutions.

4.3.2. *Janssen et al. (2003) solution*
For the near-resonance condition ($\beta\mu^{-1} = O(1)$), Janssen *et al.* (2003) derived the following governing equation for the complex amplitude of subharmonic $\hat{\xi}$ (equation (23)

therein). Using the notations of the present study, it reads as

$$\frac{d\hat{\xi}}{dx} + \hat{\xi}\left[\frac{h_x}{2h} + \frac{(k_g)_x}{2k_g} + ik_g(\frac{\mu}{2} - 1)\right] = -\frac{ik_g\hat{S}}{2\rho gh}\left(1 - \frac{2ik_g\left|\hat{S}\right|_x}{k_g\left|\hat{S}\right|} - \frac{i(k_g)_x}{k_g^2}\right) + O(\beta^2).$$

(4.14)

Recalling the expressions for the leading- and first-order forcing terms ($\hat{f}_M$ and $\hat{f}_S$; equation (3.34)), (4.14) reduces to

$$\frac{d\hat{\xi}}{dx} + \hat{\xi}\left[\frac{h_x}{2h} + \frac{(k_g)_x}{2k_g} + ik_g\left(\frac{\mu}{2} - 1\right)\right] = \frac{1}{2ik_g}(\hat{f}_M + \hat{f}_S) + O(\beta^2),$$

(4.15)

which has the solution

$$\hat{\xi}_g(x) = \int_a^x \frac{\hat{f}_M(y) + \hat{f}_S(y)}{2ik_g(y)}\sqrt{\frac{k_g(y)h(y)}{k_g(x)h(x)}}\exp\left(i\int_y^x\left(1 - \frac{\mu}{2}\right)k_g\,dx'\right)dy.$$

(4.16)

At leading order, (4.16) is equivalent to the solution of Liao *et al.* (2021) (equation (4.12) therein), which has been demonstrated above to be equivalent to the present solution (4.13).

Figure 6 shows the theoretical predictions of the amplitude and phase of group-induced subharmonic on a plane sloping bottom under the conditions of the A-4 and B-5 series in the bichromatic wave experiment of Van Noorloos (2003) using the off-resonant solution of Zou (2011), the near-resonant solutions of Liao *et al.* (2021) and Janssen *et al.* (2003) and the present solution. To compare with laboratory measurements, the free subharmonic generated due to scattering at the toe of the slope was also calculated and added to the group-induced subharmonic in figure 6 (see Appendix B for details of calculation). Note that although the component $\hat{\xi}_g^-$ is induced by upwave-propagating free subharmonics, its waveform actually propagates in the downwave direction as indicated by $\hat{\xi}_b^-$ in (3.27) and (4.9) as well as the slowly varying phase difference between $\hat{\xi}_g^-$ and the wave group (red lines in figure 6c,d). For this reason, and also because the incoming and outgoing subharmonics were separated in Van Noorloos (2003) by detecting the propagation of waveform, the component $\hat{\xi}_g^-$ should be included in the total solution $\hat{\xi}_g^+ + \hat{\xi}_{sc} + \hat{\xi}_g^-$ to compare with the incoming subharmonic in Van Noorloos (2003) (circles in figure 6).

As the water depth diminishes, the amplitude predicted by the off-resonant solution of Zou (2011) diverges as expected; the near-resonant solution of Janssen *et al.* (2003) slightly overestimated the subharmonic amplitude but underestimated the subharmonic phase lag behind the wave group. The near-resonant solution of Liao *et al.* (2021) predicts the amplitude similar to the present solution but with lower phase lag. Among the three near-resonant solutions included, the present solution agrees with laboratory measurements the best. In addition, figure 6 also indicates that in shallow water, the downwave-propagating group-induced subharmonic $\hat{\xi}_g^+$ eventually dominates the group-induced subharmonic, thus becoming the major contributor to both its amplitude and phase. Despite the dominance of $\hat{\xi}_g^+$, however, discernible discrepancy between the total solution $\hat{\xi}_g^+ + \hat{\xi}_{sc} + \hat{\xi}_g^-$ (black solid lines) and the downwave-propagating component $\hat{\xi}_g^+$ remains over the full depth range. The disagreement between experiment and theory becomes more evident at deeper water for scenario of test B-5 than A-4, due to the larger

967 A37-22

primary wave amplitude $A_1 + A_2$ and therefore the onset of wave breaking at deeper water. This is discussed further in figure 10.

4.3.3. *Contardo et al. (2021) solution*

Contardo *et al.* (2021) discretised a 1-D topography into a succession of small steps. By applying the LHS62 solution for the flat bottom on both sides of the step and applying the mass and momentum matching conditions across the step, the scattered free subharmonics induced by the wave group propagating across each single depth discontinuity were calculated. Assuming an in-phase relationship with the wave radiation stress, the initial complex amplitude of the transmitted free subharmonic is given by

$$\hat{\sigma}_{CLHRDS21}(x) = \frac{\left(\left|\hat{\xi}_{LHS62}\right|k_g h\right)\Big|_{x-\Delta x}^{x} + (k_f h)\big|_{x-\Delta x}\left(\left|\hat{\xi}_{LHS62}\right|\right)\Big|_{x-\Delta x}^{x}}{(k_f h)\big|_{x-\Delta x} + (k_f h)\big|_{x}}\frac{\hat{S}}{\left|\hat{S}\right|}, \qquad (4.17)$$

where $|_{x-\Delta x}$ and $|_x$ denote the quantities at the locations immediately before $(x - \Delta x)$ and after (x) the step respectively, corresponding to the subscripts 'sea' and 'shore' adopted by Contardo *et al.* (2021), and $|_{x-\Delta x}^{x}$ denotes the difference between the variables at x and $x - \Delta x$. The total downwave subharmonic is the superposition of the bound subharmonic as described by LHS62 and all the transmitted free subharmonics generated over the steps through which the wave groups have passed. In the case of continuous depth change, consider that the depth changes from $h(x - \Delta x)$ to $h(x)$ within a small distance Δx and then taking the limit $\Delta x \to 0$ yields

$$\hat{\sigma}_{CLHRDS21}(x) = \left[\frac{k_g + k_f}{2k_f}\frac{d\left|\hat{\xi}_{LHS62}\right|}{dx} + \frac{\left|\hat{\xi}_{LHS62}\right|}{2k_f h}\frac{d(k_g h)}{dx}\right]\frac{\hat{S}}{\left|\hat{S}\right|}, \qquad (4.18)$$

which, as shown below, is consistent with the present solution after subtracting the LHS62 solution from $\hat{\xi}_g^+$ in (4.13) at leading order.

With the phase factor $\exp(i\int^y k_g \, dx')$ in $\hat{f}_M(y)$, the phase factor of the integrand for $\hat{\xi}_g^+$ in (4.13) is $\exp(i\int^y (k_g - k_f) \, dx')$. Applying integration by parts utilising this phase factor once and combining with the LHS62 solution (3.29) reduces $\hat{\xi}_g^+$ in (4.13) to

$$\hat{\xi}_g^+(x) = \left[\hat{\xi}_{LHS62}(x) - \hat{\xi}_{LHS62}(a)\frac{\hat{\xi}_h^+(x)}{\hat{\xi}_h^+(a)}\right][1 + O(\beta)] + \int_a^x \hat{\sigma}_r(y)\frac{\hat{\xi}_h^+(x)}{\hat{\xi}_h^+(y)} \, dy, \quad (4.19)$$

where the term in the first square brackets $\hat{\xi}_{LHS62}(a)\hat{\xi}_h^+(x)/\hat{\xi}_h^+(a)$ appears due to boundary condition $\hat{\xi}_g^+(a) = 0$ and the residual source field $\hat{\sigma}_r$ due to the subtraction of the LHS62 solution is

$$\hat{\sigma}_r = \left\{\frac{k_g + k_f}{2k_f}\frac{d\left|\hat{\xi}_{LHS62}\right|}{dx} + \frac{\left|\hat{\xi}_{LHS62}\right|}{2k_f h}\frac{d(k_g h)}{dx}[1 + O(\beta)]\right\}\frac{\hat{S}}{\left|\hat{S}\right|}, \qquad (4.20)$$

which is the same as $\hat{\sigma}_{CLHRDS21}$ in (4.18) at leading order.

The present unified solution of group-induced subharmonic (3.11) reduces to the existing solutions as summarised in figure 7.
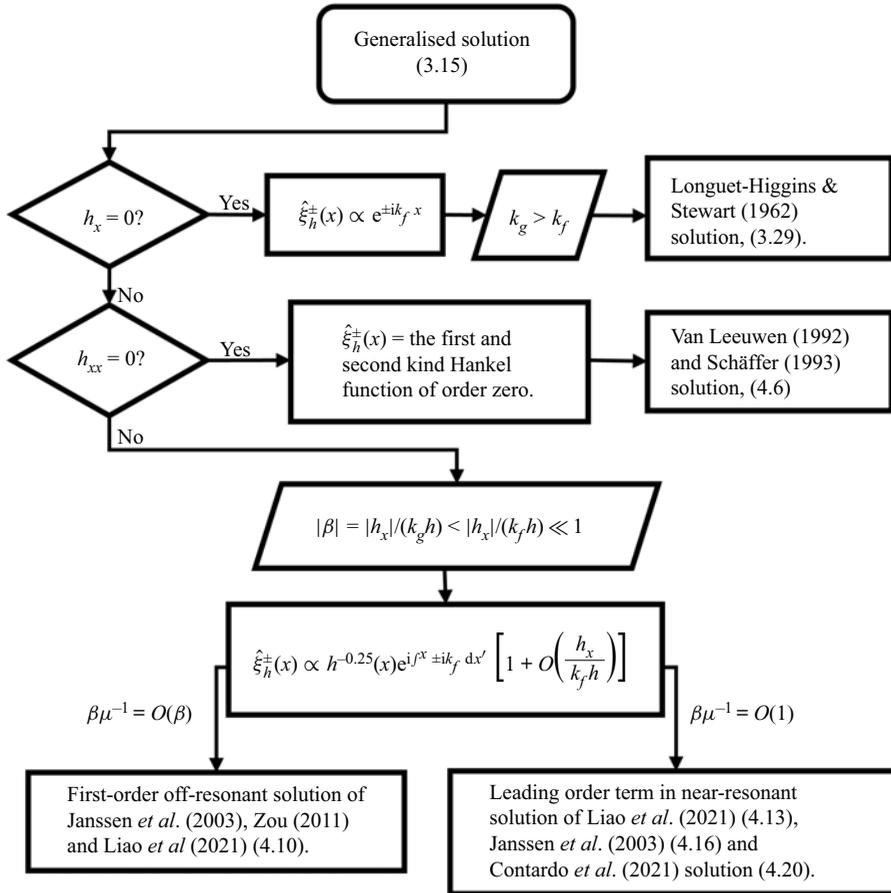
Figure 7. The present generalised solution based on Green's function (3.15) of group-induced subharmonic reduces to the solution over a flat bottom (Longuet-Higgins & Stewart 1962), a variable bottom (Zou 2011) at off-resonant condition of intermediate water, a variable bottom at near-resonant condition of shallow water (Janssen *et al.* 2003; Contardo *et al.* 2021; Liao *et al.* 2021) and over a plane beach (Van Leeuwen 1992; Schäffer 1993). Here $k_g = \omega_g/c_g$ and $k_f = \omega_g/\sqrt{gh}$ are the wavenumber of the wave group and free subharmonic propagating at the speed of shallow-water wave; $\mu = 1 - k_f^2/k_g^2$ is the degree of departure from resonance; and $\hat{\xi}_h^+(x)$ and $\hat{\xi}_h^-(x)$ are the linearly independent homogeneous solutions of (2.16) that describe the downwave- and upwave-propagating free subharmonics, respectively.

5. Effect of moving-breakpoint forcing

As long as the forcing term $\hat{f}$ for breaking waves can be theoretically pre-described, the present solution of group-induced subharmonic (3.11) can, in principle, be applied to the surf zone, assuming negligible nonlinearity of the subharmonic so that the linearised shallow-water equation is valid. As the first step, the present solution is combined with the seminal moving-breakpoint forcing model (Symonds *et al.* 1982; Schäffer 1993; Contardo & Symonds 2016). The sum of downwave and upwave components instead of individual components was solved in previous moving-breakpoint models. In contrast, these two components are independently described in the present model; therefore, the spatial evolution of the downwave component in the excursion region of moving breakpoint can be examined.
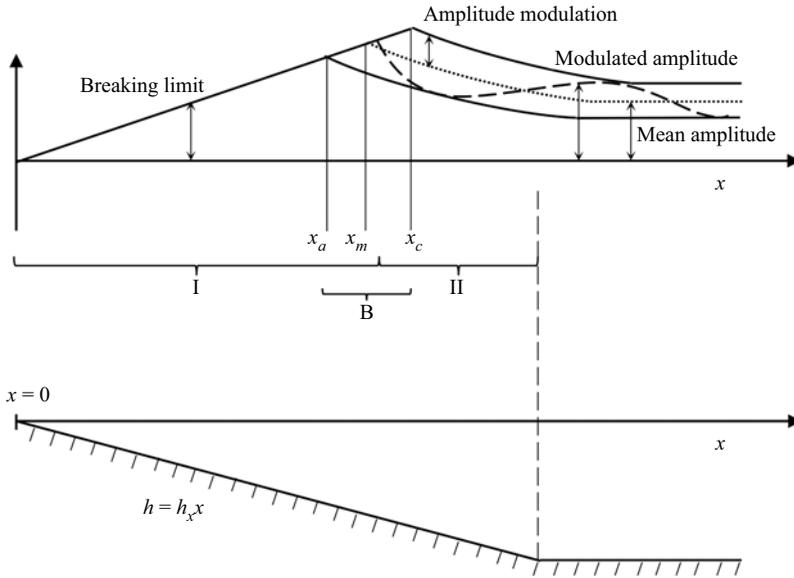
967 A37-24

Figure 8. Sketch of bottom topography and spatial variation of the amplitude of bichromatic waves normally incident on a plane sloping bottom. Positions x_a, x_m and x_c are where waves with the minimum, mean and maximum amplitude break. Reproduced from figure 3 in Schäffer (1993).

In the surf zone , the energy conservation equation (2.7) and the corresponding radiation stress solution (2.10)–(2.11) are no longer valid due to significant breaking-induced dissipation. Following Schäffer (1993), we consider weakly modulated bichromatic wave groups (modulation rate $\delta = A_2/A_1 \ll 1$ is the ratio of amplitudes of two components of bichromatic waves) normally incident onto a plane sloping bottom (figure 8). Let x_a and x_c be the horizontal coordinates of the boundaries of the moving-breakpoint region B in figure 8, and the groupiness is assumed to vanish shoreward of region B. At x_c, waves with the maximum amplitude $A_1(1 + \delta)$ start to break, i.e.

$$h(x_c) = 2\sqrt{2}A_1(x_c)(1 + \delta)/\gamma, \tag{5.1}$$

where $\gamma = $ significant wave height/depth at breakpoint is the breaker index that ranges between 0.5 and 1 (Goda 2010). Similarly, at x_a, waves with the minimum amplitude $A_1(1 - \delta)$ start to break, i.e.

$$h(x_a) = 2\sqrt{2}A_1(x_a)(1 - \delta)/\gamma. \tag{5.2}$$

The steady components of radiation stress in the surf zone and shoaling zone indicated by regions I and II in figure 8 are

$$\bar{S}^{(I)} = \frac{1}{16}\rho g\gamma^2 h^2 \left(\frac{2c_g}{c} - \frac{1}{2}\right), \quad \bar{S}^{(II)} = \frac{1}{2}\rho g A_1^2(1 + \delta^2) \left(\frac{2c_g}{c} - \frac{1}{2}\right). \tag{5.3a,b}$$

To leading order of $O(\delta)$, Schäffer (1993) derived the complex amplitude of the radiation stress gradient oscillating with group frequency in the moving-breakpoint region B:

$$\frac{d\hat{S}^{(B)}}{dx} = \frac{2}{\pi} \left(\frac{d\bar{S}^{(I)}}{dx} - \frac{d\bar{S}^{(II)}}{dx}\right) \sin\tau + O(\delta), \tag{5.4}$$

967 A37-25

where $0 \leq \tau(x) \leq \pi$ denotes the group phase when wave breaking ceases and is given by

$$2\sqrt{2}A_1(x)\{1 + \delta \cos[\tau(x)] + O(\delta^2)\} = \gamma h(x). \tag{5.5}$$

The spatial evolution of A_1 and A_2 during energy conservative shoaling can be solved from (2.8*a,b*) as

$$\frac{A_1(x)}{A_1(x_a)} = \frac{A_2(x)}{A_2(x_a)} = \sqrt{\frac{c_g(x_a)}{c_g(x)}}, \tag{5.6}$$

and therefore $\delta = A_2/A_1$ remains spatially invariant.

Substituting (5.1) and (5.2) into (5.5) yields $\tau(x_a) = \pi$ and $\tau(x_c) = 0$. In addition, at $x = x_m$ where the primary component of the bichromatic wave breaks, we have $2\sqrt{2}A_1(x_m) = \gamma h(x_m)$ and $\tau(x_m) = \pi/2$ according to (5.5).

The derivative of (5.4) gives the forcing term for governing equation of the subharmonic:

$$\frac{\mathrm{d}^2\hat{S}^{(B)}}{\mathrm{d}x^2} = \frac{2}{\pi}\left(\frac{\mathrm{d}^2\bar{S}^{(I)}}{dx^2} - \frac{\mathrm{d}^2\bar{S}^{(II)}}{dx^2}\right)\sin\tau + \frac{2}{\pi}\left(\frac{\mathrm{d}\bar{S}^{(I)}}{\mathrm{d}x} - \frac{\mathrm{d}\bar{S}^{(II)}}{\mathrm{d}x}\right)\cos\tau\frac{\mathrm{d}\tau}{\mathrm{d}x}, \tag{5.7}$$

where $\mathrm{d}\tau/\mathrm{d}x$ can be obtained from the derivatives of (5.5) and (5.6):

$$\frac{\mathrm{d}\tau}{\mathrm{d}x} = -\frac{\gamma h_x}{2\sqrt{2}A_1\delta \sin\tau}\left(\frac{h}{2c_g}\frac{\mathrm{d}c_g}{\mathrm{d}h} + 1\right) + O(\delta). \tag{5.8}$$

Positive and negative $\mathrm{d}^2\hat{S}^{(B)}/\mathrm{d}x^2$ indicate the forcing term is in phase or antiphase with the wave group at x_c, because the excursion of region B was small, and the group phase variation was neglected.

Substituting the shallow-water approximation $c_g \approx c \approx \sqrt{gh}$ and (5.8) into (5.7) yields

$$\frac{8\pi}{3\rho g\gamma^2 h_x^2}\frac{\mathrm{d}^2\hat{S}_1^{(B)}}{\mathrm{d}x^2} = \left[1 - 3\left(\frac{A_1}{\gamma h}\right)^2\right]\sin\tau + \frac{5\sqrt{2}}{16}\frac{\gamma h}{A_1\delta}\left[1 + 2\left(\frac{A_1}{\gamma h}\right)^2\right](-\cot\tau). \tag{5.9}$$

The second term on the right-hand side in (5.9) is of leading order $O(\delta^{-1})$, thus determining the sign of $\mathrm{d}^2\hat{S}^{(B)}/\mathrm{d}x^2$. In the outer half of region B ($x_m < x < x_c$), $0 < \tau < \pi/2$ and $-\cot\tau < 0$, hence $\mathrm{d}^2\hat{S}^{(B)}/\mathrm{d}x^2 < 0$; in the inner half ($x_a < x < x_m$), $\pi/2 < \tau < \pi$ and $-\cot\tau > 0$, hence $\mathrm{d}^2\hat{S}^{(B)}/\mathrm{d}x^2 > 0$. According to (3.34), at leading order, $\mathrm{d}^2\hat{S}/\mathrm{d}x^2$ prior to breaking is in antiphase with the wave group, and the above result indicates that the opposite is true once wave groups pass x_m. Therefore, the subharmonic locally generated in region B ($\hat{\xi}_{(B)}^+$) interferes with the subharmonic entering region B constructively seaward of x_m, but destructively shoreward of x_m (figure 9).

The overall effect of group forcing in region B depends on the spatial variation of the source field magnitude. Substituting (5.9) into (3.2), (3.36) and (3.7), the source field in
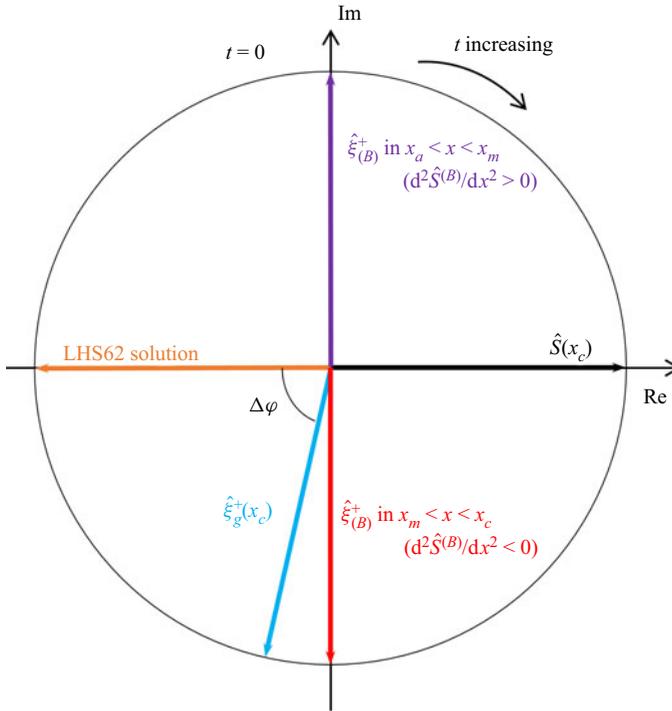
967 A37-26

Figure 9. Diagram of phase difference between the downwave-propagating subharmonic ($\hat{\xi}_g^+$) entering the moving-breakpoint region B in figure 8 at $x = x_c$ and the downwave component generated in region B ($\hat{\xi}_{(B)}^+$). Here $\Delta\varphi \leq \pi/2$ denotes a certain phase lag between $\hat{\xi}_g^+(x_c)$ and radiation stress in addition to π, which is developed during shoaling prior to breaking.

region B, $\hat{\sigma}^{(B)}$, is given by

$$\frac{64\pi}{15ih_x^2}\hat{\sigma}^{(B)} = \frac{\gamma^2}{\delta}\frac{1}{k_f h}\left(\frac{\gamma h}{2\sqrt{2}A_1} + \frac{1}{4}\frac{2\sqrt{2}A_1}{\gamma h}\right)(-\cot\tau) + O(1). \qquad (5.10)$$

Given that $A_1 \propto c_g^{-0.5} \propto h^{-1/4}$ (5.6) and $2\sqrt{2}A_1(x_m) = \gamma h(x_m)$, the coefficient of $-\cot\tau$ in the above equation reduces to

$$\frac{1}{k_f h}\left(\frac{\gamma h}{2\sqrt{2}A_1} + \frac{1}{4}\frac{2\sqrt{2}A_1}{\gamma h}\right) = \frac{1}{\omega_g}\sqrt{\frac{g}{h(x_m)}}\left\{\left[\frac{h}{h(x_m)}\right]^{3/4} + \frac{1}{4}\left[\frac{h}{h(x_m)}\right]^{-7/4}\right\}. \qquad (5.11)$$

Because $\gamma h/(2\sqrt{2}A_1) = [A_1(x_m)/h(x_m)]/(A_1/h) = [h/h(x_m)]^{5/4}$ and $\gamma h \geqslant 2\sqrt{2}A_1$ $(1-\delta)$, for $\delta < 0.23$, we have $h/h(x_m) = (\gamma h/2\sqrt{2}A_1)^{4/5} \geq (1-\delta)^{4/5} > 0.81$ and (5.11) decreases with decreasing depth. Thus the source field $\hat{\sigma}^{(B)}$ is stronger in the outer than in the inner half of region B; therefore, the downwave subharmonic is slightly enhanced over region B.

As an example of applying the present solution to the moving-breakpoint forcing model, the present solution shown in figure 6 is re-calculated here with the forcing term in region B replaced by $d^2\hat{S}^{(B)}/dx^2$ in (5.7) and the results are shown as dashed lines in figure 10 (see Appendix B for details of calculation). Note that $\hat{\xi}_g^-(x)$ in region shoreward of x_a is set to zero because the present model assumes zero groupiness and hence zero group forcing in
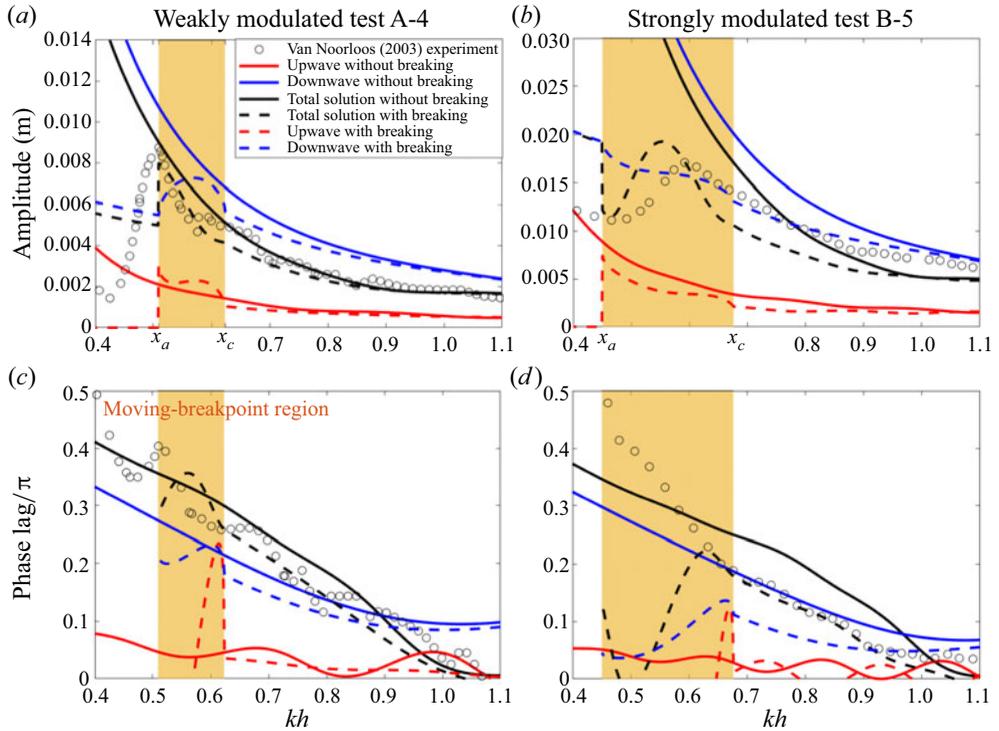
Figure 10. Amplitude (a,b) and phase (c,d) of the complex amplitude $\hat{\xi}(x)$ of the subharmonic surface elevation $\tilde{\xi}(x, t)$ induced by bichromatic wave groups normally incident over a plane sloping bottom. Weakly modulated test case A-4 (a,c) and strongly modulated test case B-5 (b,d) of the flume experiment of Van Noorloos (2003). Laboratory measurements (circles), the present solution for non-breaking wave $\hat{\xi} = \hat{\xi}_g^+ + \hat{\xi}_{sc} + \hat{\xi}_g^-$ where $\hat{\xi}_{sc}$ denotes the downwave free subharmonic generated due to scattering at the slope toe ((B11), black solid lines) and its downwave- and upwave-propagating group-induced subharmonic components, $\hat{\xi}_g^+$ (blue solid lines) and $\hat{\xi}_g^-$ (red solid lines) in (B13). The counterpart solution combined with moving-breakpoint forcing model for breaking waves is shown as dashed lines. The yellow shaded area denotes the moving breakpoint within $[x_a, x_c]$. Phase is the phase lag behind wave groups plus π. Note that in (b), the phase of the upwave component $\hat{\xi}_g^-$ was manually shifted by π for plotting purposes.

this region; therefore theoretically no upwave-propagating component of group-induced subharmonic exists. For the same reason, no phase lag was calculated shoreward of x_a where there is no wave group.

In both the weakly and strongly modulated test cases, the present solution predicts the spatial variation of the subharmonic amplitude to be in good agreement with observation, despite that the model was developed for weak modulation initially. As the water depth decreases, the predicted amplitude of the downwave-propagating subharmonic in test A-4 first increases in the outer half of the moving-breakpoint region and then decreases in the inner half by almost the same amount. The trend of the spatial evolution of amplitude is consistent with the analysis above for (5.9) in the case of the weak modulation in test A-4. For the strong modulation case of test B-5, the amplitude of the downwave-propagating component keeps increasing in the moving-breakpoint region. The predicted phase lag between the subharmonic and group deviates from observation in the moving-breakpoint region, possibly due to growing discrepancy between theoretical predictions of the wave group and observations in the surf zone. It is well known that wave groupiness is

subject to drastic change after wave breaking, possibly due to greater decay of higher waves (Svendsen & Veeramony 2001) or the modulation of breaking water depth by group-induced subharmonics (Janssen *et al.* 2003; Liu & Li 2018). Accurate estimation of the wave group phase from observations inside the surf zone would improve the prediction of phase lag. Albeit minor compared to the breaking effect, partial reflections of downwave-propagating components may also be included to further improve the accuracy of theoretical predictions (Contardo *et al.* 2023).

6. Future work

The exact form of the solution (3.11) directly relies on the spectral expression for the radiation stress, which is not well established for irregular waves in the surf zone. For bichromatic waves, (2.1) combined with the concept of breaker index results in the steady component of radiation stress solution in the surf zone $\bar{S}^{(I)}$ in (5.3*a*) used in the moving-breakpoint forcing model. This approach does not account for the effect of surface rollers, and therefore can be erroneous. For instance, for plunging-type wave breaking, there is little change in the radiation stress between the breakpoint and the plunge point (Bowen, Inman & Simmons 1968), indicating that the radiation stress in the outer surf zone does not decrease with depth as quickly as what is predicted by $\bar{S}^{(I)} \propto h^2$ in (5.3*a*,*b*). Accordingly, $\mathrm{d}\bar{S}^{(I)}/\mathrm{d}\,x$ in (5.7) can be overestimated, as can the growth of downwave-propagating subharmonic in the outer half of the moving-breakpoint region. Similarly, Rijnsdorp, Smit & Zijlema (2014) found that a non-hydrostatic model incapable of reproducing surface rollers tends to over-predict the amplitude of the subharmonic in the moving-breakpoint region. Zou *et al.* (2006) derived a generalised analytical solution for the vertical distribution of wave radiation stress in the presence of bottom slope, bottom friction and depth-induced wave breaking in the shoaling region and surf zone and conducted field observations to verify the theory. The cross-shore evolution of wave energy is described by the wave energy flux conservation equation including dissipation due to bottom friction and breaking in analogy with a travelling bore as in Thornton & Guza (1983). Existing models that account for the surface roller effect, such as those of Svendsen (1984) and Dally & Brown (1995), only consider the steady component of radiation stress that is not responsible for driving the subharmonic. Moreover, despite some efforts (e.g. Reniers *et al.* 2002; Contardo & Symonds 2016), the extension of the spectral expression of radiation stress from bichromatic to irregular wave groups in the surf zone is not as straightforward as it is for non-breaking waves. Future work of spectral expression of radiation stress for realistic irregular waves in the surf zone is needed, based on high-resolution datasets of velocity profiles from numerical or physical experiments, as per Ting & Kirby (1994), Chang & Liu (1999), Lin & Liu (1998), Wang, Zou & Reeve (2009), Kimmoun & Branger (2007), Bakhtyar *et al.* (2010), Pedrozo-Acuña *et al.* (2010), Ruju, Lara & Losada (2012), Na, Chang & Lim (2020) and Xie & Lin (2022).

In the present theoretical study, the linearised shallow-water equation is used in combination with the moving-breakpoint forcing model for the surf zone. It is necessary to adopt the fully nonlinear shallow-water equation in the nearshore region near the shoreline, where the self-interaction of the subharmonic may lead to energy dissipation in the infragravity band by transferring energy back to the short-wave band (De Bakker *et al.* 2015, 2016) or even by breaking (Van Dongeren *et al.* 2007). Moreover, subharmonics may also gain energy in the inner surf zone through bore merging by modulating the celerity of individual bores (Bonneton & Dupuis 2001; Sénéchal *et al.* 2001; Tissier *et al.* 2015), which is highly nonlinear.

The present Green's function-based solution has the potential advantage for practical application in that the Green's function for a certain area is only a function of the whole topography within that area regardless of wave conditions. The local Green's function can be extracted from *in situ* datasets through data-driven deep learning (Gin *et al.* 2021; Boullé, Earls & Townsend 2022) and then used for fast forecasts for any incident wave conditions and group forcing. Furthermore, the forcing term (3.2) can be extended to account for forcing factors other than radiation stress in governing equation (2.16) and then substituted into (3.4).

The present 1-D solution can be extended to two-dimensional wave fields by incorporating two-dimensional radiation stress and replacing the present Green's function for the 1-D shallow-water equation with the two-dimensional counterpart.

7. Conclusions

The unified solution for wave-group-induced subharmonics is derived based on Green's function, which allows for a new physical interpretation of the generation and formation of the subharmonic. The group-forcing field is divided into successive time-dependent pulses in space. The group-induced subharmonic is the superposition of all the free subharmonics generated by each group-forcing pulse, which is bound to the wave group through the group forcing related to wave radiation stress, so-called bound subharmonic infragravity wave in previous studies. The present solution reduces to the existing solutions for the off-resonance condition at intermediate water (Longuet-Higgins & Stewart 1962; Zou 2011) and the near-resonance condition at shallow water and a plane beach (Van Leeuwen 1992; Schäffer 1993; Janssen *et al.* 2003; Contardo *et al.* 2021; Liao *et al.* 2021). The underlying mechanism of the transition between bound and free subharmonics is elucidated consistently from intermediate to shallow water.

The solution based on Green's function indicates that, under the local forcing of radiation stress gradient, two subharmonics keep radiating away from the source location regardless of depth gradient considered in Contardo *et al.* (2021). As a result, downwave- and upwave-propagating subharmonic components are generated at the upwave and downwave side of any observation position. Thus, the group-induced subharmonic is dependent on the entire topography surrounding the observation position. The integrated historic topographic effect may not be significant for the off-resonance condition at intermediate water due to destructive interference among subharmonic components, but becomes significant for the downwave-propagating component for the near-resonance condition at shallow water due to constructive interference among subharmonic components.

For mildly sloping uneven bottoms, at leading order, each subharmonic is initially ahead of wave groups by $\pi/2$. For full resonance condition in shallow water, the phase difference of $\pi/2$ between downwave-propagating subharmonic and wave groups remains invariant during propagation due to the same propagating speed; thereby all the downwave-propagating subharmonics interfere with each other constructively. Consequently, the superposed downwave-propagating subharmonic leads wave groups by $\pi/2$, and its amplitude increases with travel distance of wave groups. Moreover, under this condition, the bound subharmonic is theoretically indistinguishable from the free subharmonic in the downwave-propagating subharmonic (3.30), which can be interpreted as its release. However, the opposite is true for the upwave-propagating subharmonic since resonance does not occur in the upwave direction.

For bichromatic waves normally incident on a plane beach, the amplitude of group-induced subharmonic in the moving-breakpoint region predicted by the Green's function-based solution is consistent with previous laboratory observations. For weakly modulated waves, the solution indicates that the amplitude of the downwave-propagating component increases and decreases in the outer and inner half of the moving-breakpoint region. The solution is expected to be applicable to random waves in the surf zone, as long as the spectral expression of the group forcing of breaking waves can be pre-described. This calls for further studies of the temporal and spatial variation of radiation stress in the surf zone.

Author ORCIDs.

Zhiling Liao https://orcid.org/0000-0002-2577-3822;

Qingping Zou https://orcid.org/0000-0002-5332-0855;

Ye Liu https://orcid.org/0000-0001-8993-7315;

Stephanie Contardo https://orcid.org/0000-0003-2994-8789;

Shaowu Li https://orcid.org/0000-0002-5633-9201.

Author contributions. Z.L.: theory derivation and figures; Z.L. and Q.Z.: conceptualisation and methodology; Z.L., Y.L., S.C. and Q.Z.: writing, review and editing; Q.Z. and S.L: supervision and funding.

Appendix A. Error of the solution on slowly varying water depth

The error of the solution for the bound subharmonic $\hat{\hat{\xi}}_b = \hat{\hat{\xi}}_b^+ + \hat{\hat{\xi}}_b^-$ using (3.39) is analysed as follows. The solution (3.39) for $\hat{\hat{\xi}}_b^\pm$ satisfies the following equation:

$$\frac{1}{h}\frac{d}{dx}\left(h\frac{d\hat{\hat{\xi}}_b^\pm}{dx}\right) + k_f^2\hat{\hat{\xi}}_b^\pm = \frac{1}{2}\hat{f} - \frac{1}{2}\hat{f}_r - 0.25\frac{h_{xx}}{h}\hat{\hat{\xi}}_b^\pm + 0.0625\left(\frac{h_x}{h}\right)^2\hat{\hat{\xi}}_b^\pm, \qquad (A1)$$

where $\hat{f}_r$ is the forcing term of order $O(\beta^2)$ defined in (3.34). Using (A1), $\hat{\hat{\xi}}_b = \hat{\hat{\xi}}_b^+ + \hat{\hat{\xi}}_b^-$ satisfies

$$\frac{1}{h}\frac{d}{dx}\left(h\frac{d\hat{\hat{\xi}}_b}{dx}\right) + k_f^2\hat{\hat{\xi}}_b = \hat{f} - \hat{f}_r - 0.25\frac{h_{xx}}{h}\hat{\hat{\xi}}_b + 0.0625\left(\frac{h_x}{h}\right)^2\hat{\hat{\xi}}_b. \qquad (A2)$$

Let $\hat{\hat{\xi}}_r$ be the truncated error between $\hat{\hat{\xi}}_b$ and exact solution, i.e.

$$\frac{1}{h}\frac{d}{dx}\left[h\frac{d}{dx}(\hat{\hat{\xi}}_b + \hat{\hat{\xi}}_r)\right] + k_f^2(\hat{\hat{\xi}}_b + \hat{\hat{\xi}}_r) = \hat{f}, \qquad (A3)$$

and subtracting (A2) from (A3) yields

$$\frac{1}{h}\frac{d}{dx}\left(h\frac{d\hat{\hat{\xi}}_r}{dx}\right) + k_f^2\hat{\hat{\xi}}_r = \hat{f}_r + 0.25\frac{h_{xx}}{h}\hat{\hat{\xi}}_b - 0.0625\left(\frac{h_x}{h}\right)^2\hat{\hat{\xi}}_b. \qquad (A4)$$

The order of the inhomogeneous term in (A4) is estimated using (3.28) and (3.34) to be

$$\hat{f}_r + 0.25\frac{h_{xx}}{h}\hat{\xi}_b - 0.0625\left(\frac{h_x}{h}\right)^2\hat{\xi}_b = \mu k_g^2\hat{\xi}_b O(\beta^2) + 0.25k_g^2\hat{\xi}_b\frac{h_{xx}}{k_g^2 h} - 0.0625k_g^2\hat{\xi}_b\beta^2$$

$$= k_g^2\hat{\xi}_b\,(1+\mu)\,O(\beta^2), \tag{A5}$$

and therefore (A4) becomes

$$\frac{1}{h}\frac{\mathrm{d}}{\mathrm{d}x}\left(h\frac{\mathrm{d}\hat{\xi}_r}{\mathrm{d}x}\right) + k_f^2\hat{\xi}_r = k_g^2\hat{\xi}_b\,(1+\mu)\,O(\beta^2). \tag{A6}$$

Equation (A6) has the same form as the governing equation (2.16), and the solution (3.28) indicates that $\hat{\xi}_r$ in (A6) is of order

$$\hat{\xi}_r = \frac{k_g^2\hat{\xi}_b\,(1+\mu)}{k_g^2\mu}O(\beta^2) = \hat{\xi}_b\left(\frac{1}{\mu}+1\right)O(\beta^2), \tag{A7}$$

which is of second order in bottom slope $O(\beta^2)$ for off-resonant condition $(\beta\mu^{-1} = O(\beta))$ in intermediated depth, and of first order in bottom slope $O(\beta)$ for near-resonant condition $(\beta\mu^{-1} = O(1))$ in shallow water.

Appendix B. Theoretical calculation of complex amplitude of subharmonic

The amplitude and phase of the complex amplitude of subharmonics $\hat{\xi}(x)$ over a plane sloping bottom are shown in figure 6, which is the sum of the group-induced subharmonic $\hat{\xi}_g(x)$ and the downwave-propagating free component due to scattering at the toe of the slope $\hat{\xi}_{sc}$, i.e.

$$\hat{\xi}(x) = \hat{\xi}_g(x) + \hat{\xi}_{sc}(x). \tag{B1}$$

Let $x = x_0$ denote the coordinate of the toe of the slope. The downwave-propagating component due to toe scattering is calculated as

$$\hat{\xi}_{sc}(x) = \hat{\xi}_{sc}(x_0)\frac{\hat{\xi}_h^+(x)}{\hat{\xi}_h^+(x_0)}, \tag{B2}$$

where the exact form of $\hat{\xi}_h^+(x)$ varies for different theoretical solutions. The boundary value $\hat{\xi}_{sc}(x_0)$ is given by equation (29) in Liao *et al.* (2021):

$$\hat{\xi}_{sc}(x_0) = \frac{\hat{\xi}_{LHS62}\beta}{0.25\beta - 2\mathrm{i}k_f/k_g} \times \left\{\left(\frac{k_f^2}{k_g^2}\frac{h}{\left|\hat{S}\right|}\frac{\mathrm{d}\left|\hat{S}\right|}{\mathrm{d}h} - 1 - \frac{h}{\mu}\frac{\mathrm{d}\mu}{\mathrm{d}h}\right)\right.$$

$$\left. + \frac{k_g}{k_f - k_g}\left[\frac{k_f^2}{k_g^2}\left(\frac{2h}{\left|\hat{S}\right|}\frac{\mathrm{d}\left|\hat{S}\right|}{\mathrm{d}h} + \frac{h}{k_g}\frac{\mathrm{d}k_g}{\mathrm{d}h}\right) - 1 - \frac{2h}{\mu}\frac{\mathrm{d}\mu}{\mathrm{d}h}\right]\right\}. \tag{B3}$$

To use the off-resonant solution of Zou ([2011](#)), $\hat{\xi}_h^+(x)$ is given by (see equations (3.9*c*)–(3.9*d*) therein)

$$\hat{\xi}_h^+(x) = h^{-0.25}(x)$$
$$\times \left\{ 1 + \frac{h^{-0.5}(x)}{2\mathrm{i}k_f} \int_{x_0}^x h^{-0.25}(x') \frac{\mathrm{d}}{\mathrm{d}x}\left[h(x') \frac{\mathrm{d}}{\mathrm{d}x} h^{-0.25}(x') \right] \mathrm{d}x' \right\} \exp\left(\mathrm{i} \int_{x_0}^x k_f \mathrm{d}x' \right).$$
(B4)

Substituting the off-resonant solution of Zou ([2011](#)) ([4.10](#)) into $\hat{\xi}_g(x)$ in ([B1](#)) yields

$$\hat{\xi}(x) = -\frac{\hat{S}}{\rho g h \mu}\left\{ 1 + \frac{\mathrm{i}\beta}{\mu}\left[\left(\frac{2h}{|\hat{S}|}\frac{\mathrm{d}|\hat{S}|}{\mathrm{d}h} + \frac{h}{k_g}\frac{\mathrm{d}k_g}{\mathrm{d}h} \right)(1-\mu) - 1 - \frac{2h}{\mu}\frac{\mathrm{d}\mu}{\mathrm{d}h} \right] \right\}$$
$$+ \hat{\xi}_{sc}(x_0)\frac{\hat{\xi}_h^+(x)}{\hat{\xi}_h^+(x_0)}.$$
(B5)

To use the near-resonant solution of Liao *et al.* ([2021](#)), $\hat{\xi}_h^+(x)$ is given by (see equation (13) therein)

$$\hat{\xi}_h^+(x) = [k_g(x)h(x)]^{-0.5}\exp\left(\mathrm{i}\int_{x_0}^x \left(1 - \frac{\mu}{2}\right)k_g \mathrm{d}x' \right).$$
(B6)

Substituting ([4.12](#)) and ([B2](#))–([B6](#)) into ([B1](#)) yields

$$\hat{\xi}(x) = \frac{\hat{\xi}_h^+(x)}{\hat{\xi}_h^+(x_0)}\left[\hat{\xi}_{sc}(x_0) + \hat{\xi}_b(x_0) + \int_{x_0}^x \frac{\hat{f}_M(y)}{2\mathrm{i}k_g(y)}\frac{\hat{\xi}_h^+(x_0)}{\hat{\xi}_h^+(y)} \mathrm{d}y \right],$$
(B7)

where $\hat{\xi}_b(x_0)$ is given by ([4.10](#)).

Comparison of ([4.16](#)) and ([4.12](#)) indicates that, to use the near-resonant solution of Janssen *et al.* ([2003](#)), we simply replace $\hat{f}_M$ in the above equation with $\hat{f}_M + \hat{f}_S$, i.e.

$$\hat{\xi}(x) = \frac{\hat{\xi}_h^+(x)}{\hat{\xi}_h^+(x_0)}\left[\hat{\xi}_{sc}(x_0) + \hat{\xi}_b(x_0) + \int_{x_0}^x \frac{\hat{f}_M(y) + \hat{f}_S(y)}{2\mathrm{i}k_g(y)}\frac{\hat{\xi}_h^+(x_0)}{\hat{\xi}_h^+(y)} \mathrm{d}y \right].$$
(B8)

To use the present solution, $\hat{\xi}_h^+(x)$ is replaced by ([3.35](#)), i.e.

$$\hat{\xi}_h^+(x) = [h(x)]^{-0.25}\exp\left(\mathrm{i}\int_{x_0}^x k_f \mathrm{d}x' \right).$$
(B9)

The present solution ([3.16](#)) is calculated by replacing a with x_0, with $\hat{\xi}_h^\pm$ given by ([3.35](#)) and $\hat{\xi}_f^\pm(x_0)$ given by $\hat{\xi}_b^\pm(x_0)$ in ([4.8](#)). According to the analysis in §[4.3.1](#), the present solution ([3.39](#)) is accurate to leading order for the near-resonance condition.

Hence according to (3.32) and (3.36), the source field (3.7) to leading order is

$$\hat{\sigma} = \frac{\hat{f}_M}{2\mathrm{i}k_f}. \tag{B10}$$

Therefore, the expression of solution (3.16) for the calculation in figure 6 is given by

$$\hat{\xi}(x) = \hat{\xi}_{sc}(x) + \hat{\xi}_b^+(x_0)\frac{\hat{\xi}_h^+(x)}{\hat{\xi}_h^+(x_0)} + \hat{\xi}_b^-(x_0)\frac{\hat{\xi}_h^-(x)}{\hat{\xi}_h^-(x_0)} + \int_{x_0}^x \frac{\hat{f}_M(y)}{2\mathrm{i}k_f(y)}\left[\frac{\hat{\xi}_h^+(x)}{\hat{\xi}_h^+(y)} - \frac{\hat{\xi}_h^-(x)}{\hat{\xi}_h^-(y)}\right]\,\mathrm{d}y, \tag{B11}$$

where

$$\hat{\xi}(x) = \hat{\xi}_{sc}(x) + \hat{\xi}_g^+(x) + \hat{\xi}_g^-(x), \tag{B12}$$

with $\hat{\xi}_g^+(x)$ and $\hat{\xi}_g^-(x)$ being

$$\left.\begin{aligned}
\hat{\xi}_g^+(x) &= \hat{\xi}_b^+(x_0)\frac{\hat{\xi}_h^+(x)}{\hat{\xi}_h^+(x_0)} + \int_{x_0}^x \frac{\hat{f}_M(y)}{2\mathrm{i}k_f(y)}\frac{\hat{\xi}_h^+(x)}{\hat{\xi}_h^+(y)}\,\mathrm{d}y, \\[2mm]
\hat{\xi}_g^-(x) &= \hat{\xi}_b^-(x_0)\frac{\hat{\xi}_h^-(x)}{\hat{\xi}_h^-(x_0)} - \int_{x_0}^x \frac{\hat{f}_M(y)}{2\mathrm{i}k_f(y)}\frac{\hat{\xi}_h^-(x)}{\hat{\xi}_h^-(y)}\,\mathrm{d}y.
\end{aligned}\right\} \tag{B13}$$

Combined with the moving-breakpoint forcing model, the present solution is applied to test A-4 in the experiment of Van Noorloos (2003). Region B $[x_a, x_c]$ is first identified as shown in figure 11. Then, according to (5.5), the amplitudes of bichromatic waves, $A_1(x_a)$ and $A_1(x_c)$, are estimated as $\gamma h/[2\sqrt{2}(1-\delta)]$ and $\gamma h/[2\sqrt{2}(1+\delta)]$ assuming $A_1(x)$ varies linearly from $A_1(x_0) = 0.06$ m to $A_1(x_a)$ and $A_1(x_c)$. For test B-5, the wave parameters are $[f_1, f_2] = [0.6470, 0.5005]$ Hz, $[A_1, A_2] = [0.06, 0.036]$ m, $[x_a, x_c] = [5, 10.5]$ m, $\delta = 0.6$ and $\gamma = 0.68$. Then $\hat{\xi}_g^+(x)$ and $\hat{\xi}_g^-(x)$ in region B are calculated using (B13) but now the forcing term $\hat{f}_M$ in $[x_a, x_c]$ is determined using (5.7) as

$$\hat{f}_M(x) = -\frac{1}{\rho g h}\frac{\mathrm{d}^2\hat{S}^{(B)}}{\mathrm{d}x^2}. \tag{B14}$$

Note that $\hat{\xi}_g^-(x)$ in the region shoreward of x_a is set to zero because the present model assumes zero groupiness and hence zero group forcing in this region; therefore theoretically no upwave-propagating component of group-induced subharmonic exists.

Appendix C. Generation and formation of group-induced subharmonic

Unlike previous studies, the present unified solution of group-induced subharmonic for all water depths is constructed based on Green's function. Accordingly, the group-forcing field is divided into successive pulses distributed in space, and the group-induced subharmonic is the superposition of all the free subharmonics generated by each pulse in both directions. As a result, the group-induced subharmonic is modulated by and bound to the group-forcing field and, therefore, the wave group. To understand the evolution of the subharmonic from intermediate to shallow water, the emission, propagation and interference of the free subharmonics induced by group forcing are examined in this appendix.
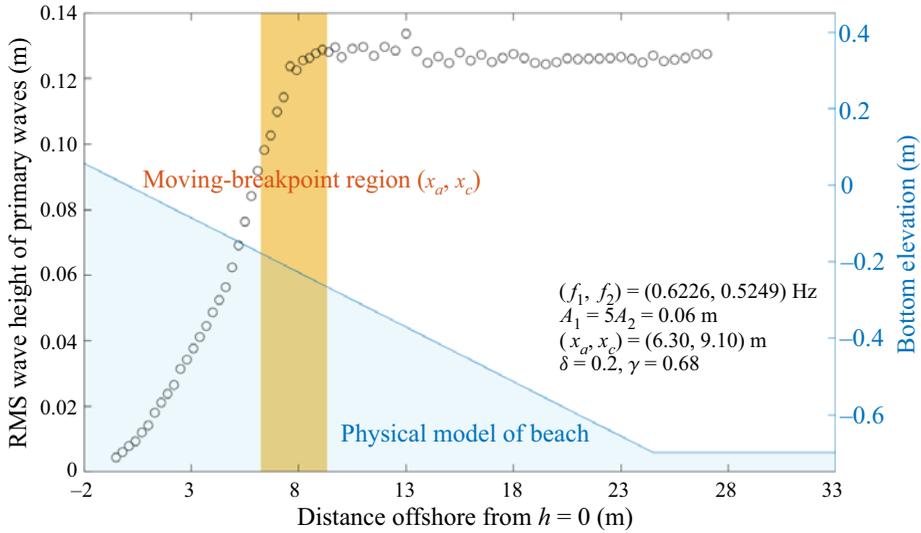
Figure 11. Left axis: the root-mean-square (RMS) wave height of primary waves of test A-4 in the experiment of Van Noorloos (2003); right axis: bottom elevation of the physical model. Parameters f_i and A_i ($i = 1, 2$) are the frequency and amplitude of the two components of bichromatic waves tested. Rate $\delta = A_2/A_1$ is the modulation rate and $\gamma =$ significant breaking height/depth is the breaker index. The seaward boundary of moving-breakpoint region x_c is where primary wave height starts to decay, and the shoreward boundary location x_a is 26.7 m from wave paddles where the smallest waves break (cf. § 5.1.1 in Van Noorloos 2003).

C.1. *Emission of free subharmonics due to group forcing*

The nonlinear short-wave group forcing of the subharmonic is represented by the radiation stress gradients $\partial^2 \tilde{S}/\partial x^2$ in the governing equation (2.14). For stationary bichromatic waves, at any given position, $\partial^2 \tilde{S}/\partial x^2$ oscillates with the period of the wave group, and so does the induced free subharmonic. The emission of the free subharmonic is described by its initial complex amplitude generated per unit distance, which constitutes the source field of group-induced subharmonic, $\hat{\sigma}$. For linear problems, the source field of the group-induced subharmonic is given by $\hat{\sigma}(y) = \hat{f}(y)G(y, y)$, where $G(y, y)$ (3.10) is the local response of surface elevation to periodic forcing with unit complex amplitude and $\hat{f}(y)$ (3.2) is the external group-forcing field with complex amplitude. Since $\hat{f}$ is modulated by wave groups, so are the initial amplitude and phase of the emitted free subharmonics.

For wave groups over continuous 1-D topography with mild sloping bottom, at leading order of bottom slope, the group forcing $\hat{f}$ is in phase with radiation stress ($\hat{f}_M$ in (3.34)) and the local response of surface elevation is $G(y, y) = 1/(2ik_f)$ (3.36), indicating that the source field is $\pi/2$ ahead of the wave groups. This phase relationship is physically understandable since, as indicated by the momentum equation (2.13), the force directly exerted onto the water body is the radiation stress gradient, which is $\pi/2$ ahead of wave groups. At leading order, the magnitude of the source field is proportional to $|\hat{\sigma}| \propto k_g^2|\hat{S}|h^{-0.5}$ (3.38), which increases with decreasing depth as $|\hat{\sigma}| \propto h^{-2}$ for a conservative shoaling process in shallow water.

C.2. *Propagation of emitted subharmonics*

For wave groups over continuous 1-D topography, under periodic group forcing, two subharmonics radiate away from the source location freely. Over a mild sloping

bottom, neglecting reflection and dissipation, the amplitude transformation of the free subharmonic from its source point y to an observation point x is described by Green's law, i.e. amplitude $\propto h^{-0.25}$. Considering the phase change from y to x, the transfer function of complex amplitude of the free subharmonic, $\hat{\sigma}(y)\,\mathrm{d}y$, is given by $[h(x)/h(y)]^{-0.25} \exp(\mathrm{i}|\int_y^x k_f\,\mathrm{d}x'|)$. As shown in § 4, this simple transfer function reduces the present solution to existing solutions for both off-resonance condition ($\beta\mu^{-1} = O(\beta)$) in intermediate depth and near-resonance condition ($\beta\mu^{-1} = O(1)$) in shallow water.

C.3. *Interference of subharmonics*

The linear superposition of all the emitted free subharmonics from each source location y yields the group-induced subharmonic at an observation point x, with complex amplitude $\hat{\xi}_g(x)$. Taking the wave group direction as the downwave direction, $\hat{\xi}_g = \hat{\xi}_g^+ + \hat{\xi}_g^-$, where $\hat{\xi}_g^+$ and $\hat{\xi}_g^-$ are the complex amplitudes of downwave- and upwave-propagating components, respectively. At leading order, the phase of the integrand in the solution for $\hat{\xi}_g^\pm$ (3.39) varies with y as $\int^y (k_g \pm k_f)\,\mathrm{d}x'$. This means that, at any observation point x, the phase of each downwave-propagating subharmonic varies slowly with its source location y as $\int^y (k_g - k_f)\,\mathrm{d}x'$, while that of the upwave-propagating subharmonic varies much faster as $\int^y (k_g + k_f)\,\mathrm{d}x'$. The phase dependence of collocated free subharmonics on their source locations determines the maximum length of the source region from which the emitted subharmonics have phases close to each other so that they interfere with each other constructively. The longer this region is, the larger the superposed subharmonic amplitude becomes. The maximum lengths of source region are of order $\pi/(k_g - k_f)$ and $\pi/(k_g + k_f)$ for the downwave- and upwave-propagating subharmonics, respectively. Consequently, the superposed amplitude of the downwave-propagating subharmonic $|\hat{\xi}_g^+|$ is about $(k_g + k_f)/(k_g - k_f)$ times $|\hat{\xi}_g^-|$, assuming that the source field is of the same order of magnitude in the entire domain. This underlying mechanism explains the stronger resonance of downwave-propagating subharmonics than upwave-propagating subharmonics.

In shallow water, near resonance occurs, i.e. $k_g \approx k_f$, and the downwave-propagating free subharmonics travel at the same speed as the source field; hence the initial phase difference of $\pi/2$ between each emitted downwave-propagating component and wave groups remains the same during propagation and so does the superposed downwave-propagating subharmonic. Moreover, all downwave-propagating subharmonics are in phase with each other and they interfere with each other constructively (figure 5). Consequently, as elucidated by (3.42), the superposed amplitude of downwave-propagating free subharmonics increases linearly with the travel distance of wave groups. In practice, however, the rate of increase with travel distance is reduced by the dissipating group forcing due to bottom friction, nonlinear energy transfer to subharmonics or depth-induced wave breaking.

Appendix D. Influence of entire topography on group-induced subharmonic

The group-induced subharmonic at any observation position includes components generated in regions on the upwave and downwave sides, meaning that the group-induced subharmonic is dependent on the whole profile of the topography. To elucidate how the local group-induced subharmonic is influenced by the topography, a conceptual model is proposed and analysed below.
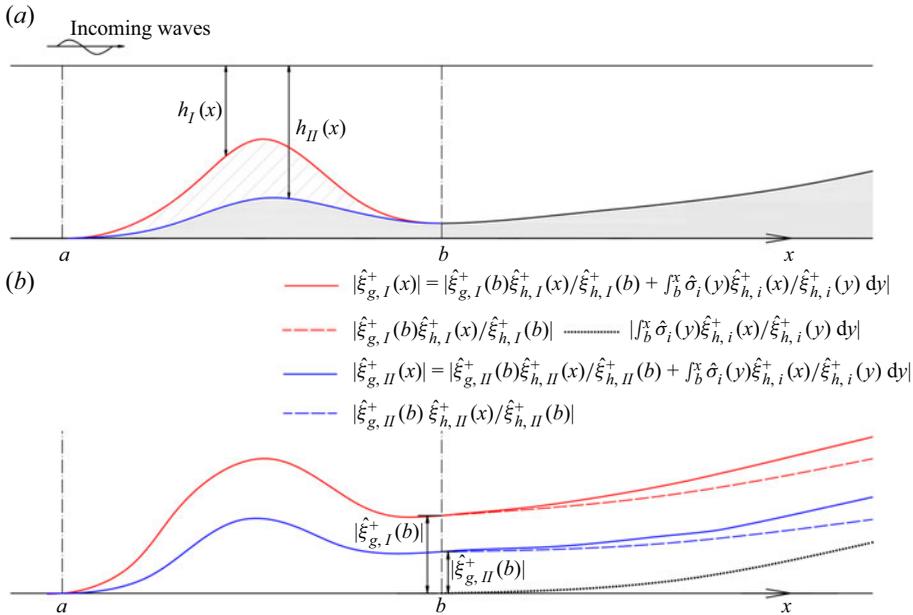
Figure 12. A conceptual model of a fixed wave train propagating from a to x over two different topographies. (*a*) Topographies $h_I(x)$ and $h_{II}(x)$, which are different in $a < x < b$ only. (*b*) Spatial evolution of the amplitude of downwave-propagating group-induced subharmonic $|\hat{\xi}_{g,i}^+(x)|$, $i = \mathrm{I, II}$ (solid lines). Here $\hat{\xi}_{g,i}^+(x)$ in $x \geqslant b$ includes two components: one is generated in $x \geqslant b$ (dotted line), which is the same for $h_I(x)$ and $h_{II}(x)$, and the other is generated in $a < x < b$ (dashed lines).

Consider a fixed wave train travelling across topographies, $h_I(x)$ and $h_{II}(x)$, with $h_I(a) = h_{II}(a)$ at the boundary $x = a$ (figure 12a). The topography is assumed to be smooth enough so that the scattering effect due to discontinuity in bottom slope or bottom curvature is negligible (Zou 2011). Let $h_I(x)$ and $h_{II}(x)$ be different in $a < x < b$ only, i.e.

$$
\left.
\begin{array}{l}
\begin{bmatrix} h_I(x) \\ \dfrac{\mathrm{d}}{\mathrm{d}x}h_I(x) \\ \dfrac{\mathrm{d}^2}{\mathrm{d}x^2}h_I(x) \end{bmatrix}
\neq
\begin{bmatrix} h_{II}(x) \\ \dfrac{\mathrm{d}}{\mathrm{d}x}h_{II}(x) \\ \dfrac{\mathrm{d}^2}{\mathrm{d}x^2}h_{II}(x) \end{bmatrix},
\quad \text{for } a < x < b, \\[2em]
\begin{bmatrix} h_I(x) \\ \dfrac{\mathrm{d}}{\mathrm{d}x}h_I(x) \\ \dfrac{\mathrm{d}^2}{\mathrm{d}x^2}h_I(x) \end{bmatrix}
\equiv
\begin{bmatrix} h_{II}(x) \\ \dfrac{\mathrm{d}}{\mathrm{d}x}h_{II}(x) \\ \dfrac{\mathrm{d}^2}{\mathrm{d}x^2}h_{II}(x) \end{bmatrix},
\quad \text{for } x \geq b.
\end{array}
\right\}
\tag{D1}
$$

The downwave-propagating group-induced subharmonic $\hat{\xi}_g^+(x)$ can be derived from (3.12a):

$$
\hat{\xi}_{g,i}^+(x) = \int_a^x \hat{\sigma}_i(y) \frac{\hat{\xi}_{h,i}^+(x)}{\hat{\xi}_{h,i}^+(y)} \, \mathrm{d}y, \quad i = \mathrm{I, II}, \tag{D2}
$$

which, in $x \geqslant b$, can be decomposed into

$$\hat{\xi}_{g,i}^+(x) = \hat{\xi}_{g,i}^+(b) \frac{\hat{\xi}_{h,i}^+(x)}{\hat{\xi}_{h,i}^+(b)} + \int_b^x \hat{\sigma}_i(y) \frac{\hat{\xi}_{h,i}^+(x)}{\hat{\xi}_{h,i}^+(y)} \, \mathrm{d}y, \quad i = \mathrm{I}, \mathrm{II}. \tag{D3}$$

Equation (D3) shows that $\hat{\xi}_g^+(x)$ in $x \geqslant b$ includes two components: the first term on the right-hand side corresponds to a free mode component generated in $a < x < b$; the second term is the component generated in the region between b and x. The influence of topography in $a < x < b$ on the group-induced subharmonic in $x \geq b$ is therefore twofold.

Firstly, topographies $h_I(x)$ and $h_{II}(x)$ in $a < x < b$ will lead to different emission and propagation processes of downwave-propagating free subharmonics induced by group forcing. Consequently, the interference pattern of these subharmonics at b is different, resulting in different subharmonics entering $x \geq b$, as shown in figure 12(b) by the different boundary values of $\hat{\xi}_{g,I}^+(b)$ and $\hat{\xi}_{g,II}^+(b)$ for $\hat{\xi}_{g,I}^+(x)$ and $\hat{\xi}_{g,II}^+(x)$ in $x \geq b$, respectively. Similarly, changing the topography on the downwave side of x can also alter the upwave-propagating component.

Secondly, the second term on the right-hand side of (D3) is also affected by the topography in $a < x < b$. On the one hand, the condition (D1) ensures that in $x \geq b$ the homogeneous solution $\hat{\xi}_{h,I}^+$ can only differ from $\hat{\xi}_{h,II}^+$ by a constant coefficient, which has no effect on $G(y, y)$ according to (3.10). On the other hand, according to (3.32), the forcing field can be expressed as

$$\hat{f}_i(x) = \frac{\hat{S}(a)}{\rho g} \left[\frac{k_{g,i}^2}{h_i} \left(-\frac{1}{k_g^2 |\hat{S}|} \frac{\mathrm{d}^2 |\hat{S}|}{\mathrm{d}x^2} - \frac{2\mathrm{i}}{k_g |\hat{S}|} \frac{\mathrm{d} |\hat{S}|}{\mathrm{d}x} - \frac{\mathrm{i}}{k_g^2} \frac{\mathrm{d}k_g}{\mathrm{d}x} + 1 \right)_i \left| \frac{\hat{S}_i(x)}{\hat{S}(a)} \right| \right]$$
$$\times \exp \left(\mathrm{i} \int_a^x k_{g,i} \, \mathrm{d}y \right), \quad i = \mathrm{I}, \mathrm{II}. \tag{D4}$$

Assuming conservation of energy flux of the primary wave, according to (2.11), $|\hat{S}|$ is only a function of water depth; hence, by (D4), $\hat{f}_i$ excluding the phase factor of wave groups is a function of water depth, bottom slope and bottom curvature, which are the same for $h_I(x)$ and $h_{II}(x)$ in $x \geq b$. The only difference between $\hat{f}_I$ and $\hat{f}_{II}$ in $x \geq b$ lies in the phase factor and is given by

$$\hat{f}_I(x) = \exp \left(\mathrm{i} \int_a^b (k_{g,I} - k_{g,II}) \, \mathrm{d}y \right) \hat{f}_{II}(x). \tag{D5}$$

This phase difference in forcing term is also the only difference between the second term of the right-hand side of $\hat{\xi}_{g,I}^+(x)$ and $\hat{\xi}_{g,II}^+(x)$ in (D3) for $x \geq b$, i.e.

$$\int_b^x \hat{\sigma}_I(y) \frac{\hat{\xi}_{h,I}^+(x)}{\hat{\xi}_{h,I}^+(y)} \, \mathrm{d}y = \exp \left(\mathrm{i} \int_a^b (k_{g,I} - k_{g,II}) \, \mathrm{d}y \right) \int_b^x \hat{\sigma}_{II}(y) \frac{\hat{\xi}_{h,II}^+(x)}{\hat{\xi}_{h,II}^+(y)} \, \mathrm{d}y. \tag{D6}$$

This is because, according to (3.7) and (3.10), the forcing term $\hat{f}_i$ is related to the source field $\hat{\sigma}_i$ through a function determined by homogeneous solutions $\hat{\xi}_{h,i}^\pm$ which are the same

967 A37-38

in $x \geq b$ for the two topographies considered. Therefore, if the condition

$$\int_a^b (k_{g,I} - k_{g,II}) \, \mathrm{d}y = 2N\pi, \quad N \in \mathbb{Z} \tag{D7}$$

is not satisfied, (D5) and (D6) show that changing the topography in $a < x < b$ shifts the phase of the downwave subharmonics generated in the subsequent region $x \geq b$ through shifting the phase of the forcing field.

The non-local influence of surrounding topography at intermediate depth is trivial due to destructive interference of the emitted free subharmonics and the source amplitude determined by radiation stress gradient decreases with water depth as mentioned in Appendix C. In shallow water, the non-local influence becomes non-trivial mainly due to the constructive interference in the full-resonance condition, but also the source amplitude is amplified at shallow water. For instance, Li *et al.* (2020) reported that, when wave groups first propagate across a shoal bathymetry, with the plateau in shallow water, and then transmit into the flat bottom zone connected to it, the transmitted subharmonic is composed of a bound subharmonic and a free subharmonic that is far more energetic than the bound subharmonic. The conceptual model discussed above based on figure 12 suggests that this is because the shallow-water region over the shoal bathymetry functions as a resonator for the downwave-propagating component that amplifies its amplitude by triggering and maintaining the constructive interference process of emitted free subharmonics. On the transmission side of the shoal, where the bottom is flat, this component keeps propagating as a free mode, coexisting with the inherent bound subharmonic described by the LHS62 solution.

It is also noteworthy that, although the group-induced subharmonic at any observation position x is essentially dependent on the entire topography on both sides of x, for practical computation, the topography and boundary value on either side are sufficient. For example, given the topography and boundary value on the upwave side of x, the solution (3.16) can be used. The effect of the topography on the downwave side of x is already included in the boundary value $\hat{\xi}_f^-(a)$ and the effect of group forcing on the upwave-propagating components is manifested by deducting the contribution of sources along the integral path from the overall effect of all sources.

List of symbols and abbreviations

a, b	boundary coordinates of an arbitrary 1-D domain $a < x < b$
A_1, A_2	amplitudes of two components of bichromatic waves
A	modulated complex amplitude of bichromatic waves
β	relative bottom slope at the wave group scale, $\beta = h_x/(k_g h)$
c	short-wave phase speed
c_g	short-wave group speed
δ	modulation rate of bichromatic waves, $\delta = A_2/A_1$
$\delta_{Dirac}(x - y)$	Dirac Delta function
E	short-wave energy
$\tilde{E}$	oscillatory component of wave energy of bichromatic wave group

$\hat{f}$	forcing term of the governing equation (2.16)
$\hat{f}_M$	main part of $\hat{f}$ at leading order of bottom slope
$\hat{f}_S$	secondary part of $\hat{f}$ at first order of bottom slope, $\hat{f}_S = \hat{f}_M O(\beta)$
$\hat{f}_r$	residual part of $\hat{f}$ due to higher-order effects of bottom slope, $\hat{f}_r = \hat{f}_M O(\beta^2)$
$\hat{f}_L$	linearised forcing term $\hat{f}$ to leading order of bottom slope, $\hat{f}_L = \hat{f}_M + \hat{f}_S$
$G(x, y)$	Green's function
g	gravitational acceleration
γ	breaking index
h	water depth
h_x	bottom slope
h_{xx}	bottom curvature
η	short-wave surface elevation
k	central wavenumber of bichromatic waves
k_g	wavenumber of bichromatic wave group, $k_g = \omega_g/c_g$
k_f	wavenumber of free mode of group-induced subharmonic, $k_f = \omega_g/\sqrt{gh}$
M	subharmonic mass flux
μ	degree of departure from resonance, $\mu = 1 - k_f^2/k_g^2$
ρ	water density
S	short-wave radiation stress
$\tilde{S}$	component of S oscillating with wave group period
$\hat{S}$	single-side complex amplitude of $\tilde{S}$
$\hat{S}^{(B)}$	$\hat{S}$ in the moving-breakpoint region (region B in figure 8)
$\bar{S}^{(I)}, \bar{S}^{(II)}$	steady component of S for breaking and non-breaking waves (regions I and II in figure 8)
$\hat{\sigma}$	source field of subharmonic due to group forcing
$\hat{\sigma}_r$	residual source field after subtracting the LHS62 bound subharmonic from group-induced subharmonic solution
$\hat{\sigma}^{(B)}$	$\hat{\sigma}$ in the moving-breakpoint region
$\hat{\sigma}_{CLHRDS21}$	residual source field $\hat{\sigma}_r$ proposed by CLHRDS21
τ	group phase when wave breaking in the moving-breakpoint region ceases
ω	central radian frequency of bichromatic waves
ω_g	radian frequency of bichromatic wave group
x_a, x_m, x_c	coordinates of the shoreward boundary, the middle point and the seaward boundary of the moving-breakpoint region
y	label of the spatial coordinate of the group-forcing field
$\tilde{\xi}$	subharmonic surface elevation
$\hat{\xi}$	single-side complex amplitude of $\tilde{\xi}$
$\hat{\xi}_g$	$\hat{\xi}$ of group-induced subharmonic
$\hat{\xi}_f$	$\hat{\xi}$ of ambient free subharmonic
$\hat{\xi}_b$	bound subharmonic in $\hat{\xi}_g$
$\hat{\xi}^+, \hat{\xi}_g^+, \hat{\xi}_f^+, \hat{\xi}_b^+, G^+$	downwave-propagating components of $\hat{\xi}, \hat{\xi}_g, \hat{\xi}_f, \hat{\xi}_b, G$ (travel in the direction of wave groups)
$\hat{\xi}^-, \hat{\xi}_g^-, \hat{\xi}_f^-, \hat{\xi}_b^-, G^-$	upwave-propagating components of $\hat{\xi}, \hat{\xi}_g, \hat{\xi}_f, \hat{\xi}_b, G$
$\hat{\xi}_h^+, \hat{\xi}_h^-$	two linearly independent homogeneous solutions of governing equation (2.16) that describe the downwave- and upwave- propagating free subharmonics, respectively
$\hat{\xi}_r$	truncated error of solution (3.39)
$\hat{\xi}_{(B)}^+$	$\hat{\xi}_g^+$ forced within the moving-breakpoint region
LHS62	Longuet-Higgins & Stewart (1962) solution for the bound subharmonic of group-induced subharmonic on flat bottom
CLHRDS21	Contardo *et al.* (2021) solution for group-induced subharmonic.

REFERENCES

BAKHTYAR, R., RAZMI, A.M., BARRY, D.A., YEGANEH-BAKHTIARY, A. & ZOU, Q. 2010 Air–water two-phase flow modeling of turbulent surf and swash zone wave motions. *Adv. Water Resour.* **33** (12), 1560–1574.

BALDOCK, T.E. 2012 Dissipation of incident forced long waves in the surf zone-Implications for the concept of "bound" wave release at short wave breaking. *Coast. Engng* **60** (1), 276–285.

BATTJES, J.A., BAKKENES, H.J., JANSSEN, T.T. & VAN DONGEREN, A.R. 2004 Shoaling of subharmonic gravity waves. *J. Geophys. Res.* **109**, C02009.

BERTIN, X., *et al.* 2018 Infragravity waves: from driving mechanisms to impacts. *Earth Sci. Rev.* **177**, 774–799.

BERTIN, X., MARTINS, K., DE BAKKER, A., CHATAIGNER, T., GUÉRIN, T., COULOMBIER, T. & DE VIRON, O. 2020 Energy transfers and reflection of infragravity waves at a dissipative beach under storm waves. *J. Geophys. Res.* **125**, e2019JC015714.

BONNETON, P. & DUPUIS, H. 2001 Transformation of irregular waves in the inner surf zone. In *International Conference on Coastal Engineering* (ed. B.L. Edge), pp. 745–754. American Society of Civil Engineers.

BOULLÉ, N., EARLS, C.J. & TOWNSEND, A. 2022 Data-driven discovery of Green's functions with human-understandable deep learning. *Sci. Rep.* **12** (1), 4824.

BOWEN, A.J., INMAN, D.L. & SIMMONS, V.P. 1968 Wave 'set-down' and set-up. *J. Geophys. Res.* **73** (8), 2569–2577.

BOWERS, E.C. 1992 Low frequency waves in intermediate water depths. In *23rd International Conference on Coastal Engineering* (ed. B.L. Edge), pp. 832–845. American Society of Civil Engineers.

BROMIRSKI, P.D., CHEN, Z., STEPHEN, R.A., GERSTOFT, P., ARCAS, D., DIEZ, A., ASTER, R.C., WIENS, D.A. & NYBLADE, A. 2017 Tsunami and infragravity waves impacting Antarctic ice shelves. *J. Geophys. Res.* **122** (7), 5786–5801.

CHANG, K.-A. & LIU, P.L.-F. 1999 Experimental investigation of turbulence generated by breaking waves in water of intermediate depth. *Phys. Fluids* **11** (11), 3390–3400.

CHERITON, O., STORLAZZI, C. & ROSENBERGER, K. 2016 Observations of wave transformation over a fringing coral reef and the importance of low-waves and offshore water levels to runup, overwash, and coastal flooding. *J. Geophys. Res.* **121**, 3121–3140.

CONTARDO, S., LOWE, R.J., DUFOIS, F., HANSEN, J.E., BUCKLEY, M. & SYMONDS, G. 2023 Free long-wave transformation in the nearshore zone through partial reflections. *J. Phys. Oceanogr.* **53**, 661–681.

CONTARDO, S., LOWE, R.J., HANSEN, J.E., RIJNSDORP, D.P., DUFOIS, F. & SYMONDS, G. 2021 Free and forced components of shoaling long waves in the absence of short-wave breaking. *J. Phys. Oceanogr.* **51** (5), 1465–1487.

CONTARDO, S. & SYMONDS, G. 2013 Infragravity response to variable wave forcing in the nearshore. *J. Geophys. Res.* **118** (12), 7095–7106.

CONTARDO, S. & SYMONDS, G. 2016 Generation of free infragravity waves by time-varying breakpoint with real wave conditions. *J. Coast. Res.* **75** (sp1), 836–840.

CONTARDO, S., SYMONDS, G. & DUFOIS, F. 2018 Breakpoint forcing revisited: phase between forcing and response. *J. Geophys. Res.* **123** (2), 1354–1363.

DALLY, W. & BROWN, C. 1995 A modeling investigation of the breaking wave roller with application to cross-shore currents. *J. Geophys. Res.* **1002**, 24873–24883.

DE BAKKER, A.T.M., HERBERS, T.H.C., SMIT, P.B., TISSIER, M.F.S. & RUESSINK, B.G. 2015 Nonlinear infragravity wave interactions on a gently sloping laboratory beach. *J. Phys. Oceanogr.* **45** (2), 589–605.

DE BAKKER, A.T.M., TISSIER, M.F.S. & RUESSINK, B.G. 2016 Beach steepness effects on nonlinear infragravity-wave interactions: a numerical study. *J. Geophys. Res.* **121** (1), 554–570.

DIAZ-HERNANDEZ, G., MENDEZ, F.J., LOSADA, I.J., CAMUS, P. & MEDINA, R. 2015 A nearshore long-term infragravity wave analysis for open harbours. *Coast. Engng* **97**, 78–90.

DUFFY, D.G. 2015 *Green's Functions with Applications*. Chapman and Hall/CRC.

ELGAR, S. & GUZA, R.T. 1985 Observations of bispectra of shoaling surface gravity waves. *J. Fluid Mech.* **161**, 425–448.

GIN, C.R., SHEA, D.E., BRUNTON, S.L. & KUTZ, J.N. 2021 DeepGreen: deep learning of Green's functions for nonlinear boundary value problems. *Sci. Rep.* **11** (1), 21614.

GODA, Y. 2010 Reanalysis of regular and random breaking wave statistics. *Coast. Engng J.* **52** (1), 71–106.

GREEN, G. 1838 On the motion of waves in a variable canal of small depth and width. *Trans. Camb. Phil.* **6**, 457.

GUÉRIN, T., DE BAKKER, A. & BERTIN, X. 2019 On the bound wave phase lag. *Fluids* **4**, 152.

HASSELMANN, K. 1962 On the non-linear energy transfer in a gravity-wave spectrum. Part 1. General theory. *J. Fluid Mech.* **12** (4), 481–500.

HENDERSON, C.S., FIEDLER, J.W., MERRIFIELD, M.A., GUZA, R.T. & YOUNG, A.P. 2022 Phase resolving runup and overtopping field validation of swash. *Coast. Engng* **175**, 104128.

INCE, E.L. 1956 *Ordinary Differential Equations*. Dover.

INCH, K., DAVIDSON, M., MASSELINK, G. & RUSSELL, P. 2017 Observations of nearshore infragravity wave dynamics under high energy swell and wind–wave conditions. *Cont. Shelf Res.* **138**, 19–31.

JANSSEN, T.T., BATTJES, J.A. & VAN DONGEREN, A.R. 2003 Long waves induced by short-wave groups over a sloping bottom. *J. Geophys. Res.* **108** (C8), 3252.

KIMMOUN, O. & BRANGER, H. 2007 A particle image velocimetry investigation on laboratory surf-zone breaking waves over a sloping beach. *J. Fluid Mech.* **588**, 353–397.

LI, S., LIAO, Z., LIU, Y. & ZOU, Q. 2020 Evolution of infragravity waves over a shoal under non-breaking conditions. *J. Geophys. Res.* **125** (8), e2019JC015864.

LIAO, Z., LI, S., LIU, Y. & ZOU, Q. 2021 An analytical spectral model for infragravity waves over topography in intermediate and shallow water under non-breaking conditions. *J. Phys. Oceanogr.* **51** (9), 2749–2765.

LIN, P. & LIU, P.L.-F. 1998 A numerical study of breaking waves in the surf zone. *J. Fluid Mech.* **359**, 239–264.

LIST, J.H. 1992 A model for the generation of two-dimensional surf beat. *J. Geophys. Res.* **97** (C4), 5623–5635.

LIU, Y. & LI, S. 2018 Variation of wave groupiness across a fringing reef. *ASCE J. Waterway Port Coastal Ocean Engng* **144** (6), 04018022.

LIU, Y.J., MUKHERJEE, S., NISHIMURA, N., SCHANZ, M., YE, W., SUTRADHAR, A., PAN, E., DUMONT, N.A., FRANGI, A. & SAEZ, A. 2011 Recent advances and emerging applications of the boundary element method. *Appl. Mech. Rev.* **64**, 030802.

LIU, Y., YAO, Y., LIAO, Z., LI, S., ZHANG, C. & ZOU, Q. 2023 Fully nonlinear investigation on energy transfer between long waves and short-wave groups over a reef. *Coast. Engng* **179**, 104240.

LONGUET-HIGGINS, M.S. & COKELET, E.D. 1976 The deformation of steep surface waves on water. I. A numerical method of computation. *Proc. R. Soc. Lond.* A **350**, 1–26.

LONGUET-HIGGINS, M.S. & STEWART, R.W. 1960 Changes in the form of short gravity waves on long waves and tidal currents. *J. Fluid Mech.* **8** (4), 565–583.

LONGUET-HIGGINS, M.S. & STEWART, R.W. 1962 Radiation stress and mass transport in gravity waves, with application to 'surf beats'. *J. Fluid Mech.* **13** (4), 481–504.

MASSELINK, G. 1995 Group bound long waves as a source of infragravity energy in the surf zone. *Cont. Shelf Res.* **15** (13), 1525–1547.

MCALLISTER, M.L., ADCOCK, T.A.A., TAYLOR, P.H. & VAN DEN BREMER, T.S. 2017 The set-down and set-up of directionally spread and crossing surface gravity wave groups. *J. Fluid Mech.* **835**, 131–169.

MEI, C.C. & BENMOUSSA, C. 1984 Long waves induced by short-wave groups over an uneven bottom. *J. Fluid Mech.* **139**, 219–235.

MELITO, L., PARLAGRECO, L., DEVOTI, S. & BROCCHINI, M. 2022 Wave- and tide-induced infragravity dynamics at an intermediate-to-dissipative microtidal beach. *J. Geophys. Res.* **127**, e2021JC017980.

MILES, J.W. 1972 Wave propagation across the continental shelf. *J. Fluid Mech.* **54**, 63–80.

MILES, J.W. 1974 Harbor seiching. *Annu. Rev. Fluid Mech.* **6**, 17–33.

MOURA, T. & BALDOCK, T. 2019 The influence of free long wave generation on the shoaling of forced infragravity waves. *J. Mar. Sci. Engng* **7**, 305.

MUNK, W.H. 1949 Surf beats. *EOS Trans. AGU* **30** (6), 849–854.

NA, B., CHANG, K.-A. & LIM, H.-J. 2020 Flow kinematics and air entrainment under laboratory spilling breaking waves. *J. Fluid Mech.* **882**, A15.

NIELSEN, P. & BALDOCK, T.E. 2010 N-shaped surf beat understood in terms of transient forced long waves. *Coast. Engng* **57** (1), 71–73.

NING, D., SHI, J., ZOU, Q. & TENG, B. 2015 Investigation of hydrodynamic performance of an OWC (oscillating water column) wave energy device using a fully nonlinear HOBEM (higher-order boundary element method). *Energy* **83**, 177–188.

PALMSTEN, M.L. & SPLINTER, K.D. 2016 Observations and simulations of wave during a laboratory dune erosion experiment. *Coast. Engng* **115**, 58–66.

PEDROZO-ACUÑA, A., TORRES-FREYERMUTH, A., ZOU, Q., HSU, T.-J. & REEVE, D.E. 2010 Diagnostic investigation of impulsive pressures induced by plunging breakers impinging on gravel beaches. *Coast. Engng* **57** (3), 252–266.

RENIERS, A.J.H.M., VAN DONGEREN, A.R., BATTJES, J.A. & THORNTON, E.B. 2002 Linear modeling of infragravity waves during delilah. *J. Geophys. Res.* **107** (C10), 3137.

RIJNSDORP, D.P., SMIT, P.B. & GUZA, R.T. 2022 A nonlinear, non-dispersive energy balance for surfzone waves: infragravity wave dynamics on a sloping beach. *J. Fluid Mech.* **944**, A45.

RIJNSDORP, D., SMIT, P. & ZIJLEMA, M. 2014 Non-hydrostatic modelling of infragravity waves under laboratory conditions. *Coast. Engng* **85**, 30–42.

ROELVINK, D., RENIERS, A., VAN DONGEREN, A.R., VAN THIEL DE VRIES, J., MCCALL, R. & LESCINSKI, J. 2009 Modelling storm impacts on beaches, dunes and barrier islands. *Coast. Engng* **56**, 1133–1152.

RUJU, A., LARA, J.L. & LOSADA, I.J. 2012 Radiation stress and low-frequency energy balance within the surf zone: a numerical approach. *Coast. Engng* **68**, 44–55.

SCHÄFFER, H.A. 1993 Infragravity waves induced by short-wave groups. *J. Fluid Mech.* **247**, 551–588.

SÉNÉCHAL, N., DUPUIS, H., BONNETON, P., HOWA, H. & PEDREROS, R. 2001 Observation of irregular wave transformation in the surf zone over a gently sloping sandy beach on the French Atlantic coastline. *Oceanol. Acta* **24** (6), 545–556.

STOCKDON, H.F., HOLMAN, R.A., HOWD, P.A. & SALLENGER, A.H. 2006 Empirical parameterization of setup, swash, and runup. *Coast. Engng* **53** (7), 573–588.

SVENDSEN, I.A. 1984 Wave heights and set-up in a surf zone. *Coast. Engng* **8** (4), 303–329.

SVENDSEN, I.A. & VEERAMONY, J. 2001 Wave breaking in wave groups. *ASCE J. Waterway Port Coastal Ocean Engng* **127** (4), 200–212.

SYMONDS, G., HUNTLEY, D.A. & BOWEN, A.J. 1982 Two-dimensional surf beat: long wave generation by a time-varying breakpoint. *J. Geophys. Res.* **87** (C1), 492–498.

TELSTE, J.G. & NOBLESSE, F. 1986 Numerical evaluation of the Green function of water-wave radiation and diffraction. *J. Ship Res.* **30**, 69–84.

THOMSON, J., ELGAR, S., RAUBENHEIMER, B., HERBERS, T.H.C. & GUZA, R.T. 2006 Tidal modulation of infragravity waves via nonlinear energy losses in the surfzone. *Geophys. Res. Lett.* **33**, L05601.

THORNTON, E.B. & GUZA, R.T. 1983 Transformation of wave height distribution. *J. Geophys. Res.* **88** (C10), 5925–5938.

TING, F.C.K. & KIRBY, J.T. 1994 Observation of undertow and turbulence in a laboratory surf zone. *Coast. Engng* **24** (1–2), 51–80.

TISSIER, M., BONNETON, P., MICHALLET, H. & RUESSINK, B.G. 2015 Infragravity-wave modulation of short-wave celerity in the surf zone. *J. Geophys. Res.* **120** (10), 6799–6814.

TUCKER, M.J. 1950 Surf beats: sea waves of 1 to 5 min. period. *Proc. R. Soc.* A **202** (1071), 565–573.

VAN DONGEREN, A., BATTJES, J.A., JANSSEN, T.T., VAN NOORLOOS, J., STEENHAUER, K., STEENBERGEN, G. & RENIERS, A. 2007 Shoaling and shoreline dissipation of low-waves. *J. Geophys. Res.* **112**, C02011.

VAN LEEUWEN, P.J. 1992 Low frequency wave generation due to breaking waves. PhD thesis, TU Delft.

VAN NOORLOOS, J.C. 2003 Energy transfer between short wave groups and bound long waves on a plane slope. Thesis, TU Delft.

VOISIN, B. 1991 Internal wave generation in uniformly stratified fluids. Part 1. Green's function and point sources. *J. Fluid Mech.* **231**, 439–480.

WANG, R., NING, D. & ZOU, Q. 2020 Wave loads on a land-based dual-chamber oscillating water column wave energy device. *Coast. Engng* **160**, 103744.

WANG, Z., ZOU, Q. & REEVE, D. 2009 Simulation of spilling breaking waves using a two phase flow CFD model. *Comput. Fluids* **38** (10), 1995–2005.

XIE, Z. & LIN, P. 2022 Eulerian and Lagrangian transport by shallow–water breaking waves. *Phys. Fluids* **34** (3), 032116.

ZHANG, Q., TOORMAN, E.A. & MONBALIU, J. 2020 Shoaling of bound infragravity waves on plane slopes for bichromatic wave conditions. *Coast. Engng* **158**, 103684.

ZHAO, X., LI, Y., ZOU, Q., HAN, D. & GENG, J. 2022 Long wave absorption by a dual purpose Helmholtz resonance OWC breakwater. *Coast. Engng* **178**, 104203.

ZHENG, Y., LIN, Z., LI, Y., ADCOCK, T.A.A., LI, Y. & VAN DEN BREMER, T.S. 2020 Fully nonlinear simulations of unidirectional extreme waves provoked by strong depth transitions: the effect of slope. *Phys. Rev. Fluids* **5**, 064804.

ZOU, Q. 2011 Generation, transformation, and scattering of long waves induced by a short-wave group over finite topography. *J. Phys. Oceanogr.* **41**, 1842–1859.

ZOU, Q., BOWEN, A.J. & HAY, A.E. 2006 Vertical distribution of wave shear stress in variable water depth: theory and field observations. *J. Geophys. Res.* **111**, C09032.